Interface problems with quadratic X-FEM: design of a stable multiplier space and error analysis

Guilhem Ferté, Patrick Massin, Nicolas Moes

Interface problems with quadratic X-FEM: design of a stable multiplier space and error analysis

G. Ferté[1,*,†], P. Massin[1] and N. Moës[2]

[1]*LaMSid, UMR EDF - CNRS - CEA, UMR 8193, EDF R&D, 1 av. du général de Gaulle, 92141 Clamart, France*
[2]*GeM Institute Ecole Centrale de Nantes, Université de Nantes - CNRS, Ecole Centrale de Nantes, 1 rue de la Noë, BP 92101, 44321 Nantes, France*

The aim of this paper is to propose a procedure to accurately compute curved interfaces problems within the extended finite element method and with quadratic elements. It is dedicated to gradient discontinuous problems, which cover the case of bimaterials as the main application. We focus on the use of Lagrange multipliers to enforce adherence at the interface, which makes this strategy applicable to cohesive laws or unilateral contact. Convergence then occurs under the condition that a discrete inf-sup condition is passed. A dedicated P1 multiplier space intended for use with P2 displacements is introduced. Analytical proof that it passes the inf-sup condition is presented in the two-dimensional case. Under the assumption that this inf-sup condition holds, a priori error estimates are derived for linear or quadratic elements as functions of the curved interface resolution and of the interpolation properties of the discrete Lagrange multipliers space. The estimates are successfully checked against several numerical experiments: disparities, when they occur, are explained in the literature. Besides, the new multiplier space is able to produce quadratic convergence from P2 displacements and quadratic geometry resolution.

KEY WORDS: extended finite element method; contact; partial differential equations

1. INTRODUCTION

Solving interface problems with the classical FEM requires a considerable meshing effort when interfaces have complex geometries. Hence, to reduce the burden of meshing, Moës, Dolbow, and Belytschko [1] proposed an extended finite element method (X-FEM) allowing surfaces of discontinuities within elements. The discontinuity is described by a local enrichment of the basis functions on crossed-through elements with discontinuous functions across the interface, abiding by the rules of the partition of unity method in [2].

In weak discontinuity problems, such as heat conduction or linear elasticity in bimaterials, a continuous field of interest is searched *but with a discontinuous gradient* across the interface. Those problems are actually more tricky to handle than strong discontinuities: although fully uncoupling, fields on either sides basically consist in doubling some DOFs around the interface and is in principle easy to implement; weak discontinuity problems bring about additional issues by demanding field continuity across the interface, which could be viewed as some *partial* uncoupling. There are basically three approaches for enforcing that continuity. The first consists in using continuous but gradient discontinuous functions across the interface. The other two consist in enforcing the continu-

*Correspondence to: G. Ferté, LaMSid, UMR EDF - CNRS - CEA, UMR 8193, EDF R&D, 1 av. du général de Gaulle, 92141 Clamart, France.
†E-mail: guilhem.ferte@edf.fr

ity in a weak sense either with Nitsche's stabilization method or with Lagrange multipliers. We shall focus on the latter approach in this paper, after giving some background details about the others.

Sukumar and coworkers [3] were the first to consider using X-FEM to account for inclusions. They would then take the absolute value of the level set function as the enrichment function. With this enrichment, they would observe suboptimal convergence rates due to poor properties on the elements « adjacent to those intersected ». They would then modify the enrichment to even the enrichment function on those elements and then almost get optimal rates. Moës and coworkers [4] then proposed a *modified abs-enrichment*, named *ridge enrichment that does not require any treatment for such* « *blending elements* » and therefore yields optimal rates. Aiming at a general method that would be applicable to other enrichment than the ridge, Fries and al [5] proposed a *corrected X-FEM* formulation, which works out the set of enriched nodes and associated shape functions rather than a specific enrichment function. Meanwhile, Legay and al [6] used enhanced strain techniques to tackle the issue, inspired from assumed strain strategies in [7, 8].

In the same article [6], the authors first used higher-order X-FEM for weak discontinuity problems without assumed strain or any other specific handling of blending elements but by multiplying the enrichment with shape functions one degree lower than those of the classical part. Finally, Cheng and Fries [9] adapted standard and *modified abs-enrichment*, as well as *corrected X-FEM* for higher orders, compared with the three and concluded that at higher orders, the corrected X-FEM would behave better than the standard one, the latter converging faster than the modified abs-enrichment.

These gradient discontinuous displacement enrichment strategies have the advantage of producing discrete solutions, which exhibit zero jump across the interface exactly, by construction of the enrichment functions. On the contrary, the multiplier approach enforces this condition weakly so that the discrete jump is not necessarily exactly zero across the interface. However, designing a gradient discontinuous enrichment that preserves optimality in blending elements even at higher orders and for curved interfaces is somehow cumbersome. This consideration motivated the first use of Lagrange multipliers to account for material interfaces in [10], which was recently further developed in [11]. The multiplier method is moreover prone to extensions to other interface laws (e.g., unilateral contact or cohesive law).

Ji and Dolbow [12] were the first to introduce Lagrange multipliers in the X-FEM. They reported that a naive discretization triggers oscillations of the multipliers and a loss of convergence and so does high-stiffness penalization. The critical point lies in a discrete inf-sup condition, which determines the stability of the formulation. In X-FEM, this condition is even more technical to verify because of the non-conformity of the mesh and is violated for a naive discretization. There are several ways to restore it in the literature, namely,

(1) An enrichment of the displacement basis with bubble function on the interface in [13–15];
(2) The definition of a reduced Lagrange multiplier space, which was improved in a sequence of three papers by Moës and al [16], Géniaut and al [17], and Béchet and al [18]. These spaces are designed for use with linear elements, and we discuss extension to quadratic elements in this paper.

These are called *stable* formulations, in that they work out the discrete spaces directly, as opposed to *stabilized* formulations, which circumvent the inf-sup condition with a modification of the variational form by

(1) An adaptation of Nitsche's approach [19] to the X-FEM by Hansbo [20], further developed by [15, 21] and [22]. In this approach, no Lagrange multiplier is introduced in the formulation: the normal flux directly plays its role and a stabilization term *on the jump* is added to avoid oscillations;
(2) The addition of a stabilization term *on the multiplier/flux discrepancy* into the weak formulation by [23, 24] based on Barbosa and Hughes approach [25]. A connection was made by Stenberg [26] between this approach and Nitsche's one [19];
(3) A three-field approach with ellipticity-enhancing terms by Gravouil and al [27].

Dealing more specifically with curved interfaces, several authors reported a loss of optimality of the convergence rate with higher-order X-FEM when approximating the interface geometry by

linear segments (see [6, 9, 28, 29]). Ranging from a geometrical description on a finer submesh ([28, 29] to curved subcells ([6, 9]), successful remedies to the problem were proposed. To say things briefly, we adopted the geometry description suggested by Legay and coworkers [6] with a higher-order level set interpolation and curved quadratic triangles as subcells.

Studying interface problems with X-FEM and Lagrange multipliers, possibly at higher orders and/or with curved interfaces, our task is threefold

(1) Design both optimal and stable reduced multiplier space suited for use together with quadratic displacements,
(2) Derive theoretical a priori estimates for *stable* formulations of X-FEM with Lagrange multipliers—to our knowledge, this has solely been done for *stabilized* formulations up to now,
(3) Include the influence of the geometry representation in those estimates.

In Section 3, the new 'P2-dedicated' discrete multiplier space is introduced. Analytical proof that it passes the stability inf-sup condition is presented in two-dimensional case. In Section 4, the description of the geometry is presented and some results are recalled about assessing its accuracy. In Section 5, the a priori estimates are derived, and hereby, the influence on the convergence rate of the aforementioned geometrical description and the interpolation properties of the multiplier space is investigated. Numerical tests are carried out in Section 6, and numerical orders are compared with their theoretical counterparts. Based on these tests, some theoretical predictions appear suboptimal, down $h^{1/2}$, but the reason for this appears documented by [30, 31]. We show, for a quadratic displacement, that the combination of a quadratic geometrical description of the interface with the new restriction algorithm yields optimal convergence *in practice*, with an order 2.

2. FORMULATION OF THE CONTINUOUS PROBLEM

We consider an elastic body occupying a domain Ω in $\mathbb{R}^2$, Ω being a bounded open set. This body is cut through by an interface Γ, which typically corresponds to a change in material properties. Domain Ω is thus split into two open sets $\Omega_i, i \in \{1,2\}$ so that $\Omega = \Omega_1 \cup \Omega_2 \cup \Gamma$ (see Figure 1), and the restriction to Ω_i of any field $\boldsymbol{v}$ is denoted $\boldsymbol{v}_i$. For each such part, the remaining of the boundary $\partial\Omega_i \backslash \Gamma$ is composed of non-overlapping parts Γ_u^i and Γ_g^i, where conditions are prescribed on the displacement $\boldsymbol{u}_i$ and the surface force distribution $\boldsymbol{g}_i$, respectively. We assume that $\forall i \in \{1,2\}, \Gamma_u^i$ has nonzero measure so as to prevent rigid body motion.

Each body is subjected to volume forces $\boldsymbol{f}_i$ in addition to the surface loads. Transformations always remain small. Equilibrium equations in Ω_i then read

$$\nabla \cdot \boldsymbol{\sigma}_i + \boldsymbol{f}_i = 0 \text{ in } \Omega_i \tag{1}$$

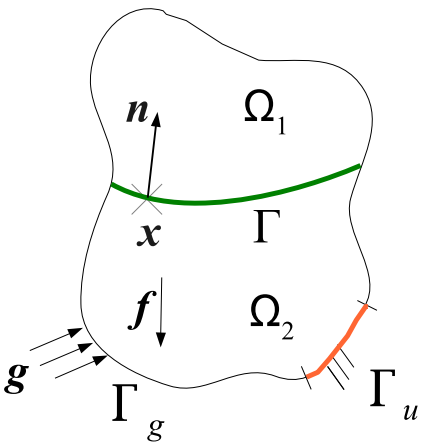

Figure 1. Definition of the problem.

$$\boldsymbol{\sigma}_i \cdot \boldsymbol{n}_i = \boldsymbol{g}_i \text{ on } \Gamma_g^i, i = 1, 2 \tag{2}$$

$$\boldsymbol{u}_i = 0 \text{ on } \Gamma_u^i \tag{3}$$

where $\boldsymbol{\sigma}_i$ is the Cauchy stress tensor, defined from the elasticity fourth-order tensor $\boldsymbol{A}_i$ and the strain tensor $\boldsymbol{\epsilon}_i = \frac{1}{2}\left(\nabla \boldsymbol{u}_i + \nabla \boldsymbol{u}_i^{\mathrm{T}}\right)$, as $\boldsymbol{\sigma}_i = \boldsymbol{A}_i \cdot \boldsymbol{\epsilon}_i$. Moreover, the continuity conditions across the interface read

$$[\boldsymbol{u}] = \boldsymbol{0} \text{ on } \Gamma \tag{4}$$

$$[\boldsymbol{\sigma} \cdot \boldsymbol{n}] = \boldsymbol{0} \text{ on } \Gamma \tag{5}$$

where for $\boldsymbol{x} \in \Gamma$, $[\boldsymbol{u}](\boldsymbol{x}) = \boldsymbol{u}_2(\boldsymbol{x}) - \boldsymbol{u}_1(\boldsymbol{x})$ is the displacement jump.

In what follows, we adopt classical notations for the functional spaces: $W^{m,p}(\Omega)$ denotes the Sobolev space of functions v for which all components of the m^{th} -order weak derivative $D^m(v)$ lie in $L^p(\Omega)$. In other words, for any multi-index $\alpha := (\alpha_1, \alpha_2) \in \mathbb{N}^2$ such that $|\alpha| := \alpha_1 + \alpha_2 \leqslant m$, it holds $\partial^\alpha v := \frac{\partial^{|\alpha|} v}{\partial x_1^{\alpha_1} \partial x_2^{\alpha_2}} \in L^p(\Omega)$. The associated semi-norm is denoted $|.|_{m,p,\Omega}$ and the associated norm $\|.\|_{m,p,\Omega}$. Classically, we note $H^m(\Omega) := W^{m,2}(\Omega)$, for which the index $p = 2$ is omitted in the notations of the associated semi-norm and norm. We also introduce product spaces $H^m(\Omega_1) \times H^m(\Omega_2)$, which are endowed with the broken norm $\|v\|^2_{m,\Omega_1 \cup \Omega_2} := \|v\|^2_{m,\Omega_1} + \|v\|^2_{m,\Omega_2}$. In this paper, C will denote a generic nonnegative constant and c a positive constant.

The components of the solution to problems (1–5) are assumed to belong to the functional space $V := \left\{v \in H^1(\Omega_1) \times H^1(\Omega_2), v|_{\Gamma_u^i} = 0, i \in \{1, 2\}, [v]|_{\partial\Gamma} = 0\right\}$, where $\partial\Gamma$ denotes the extremities of Γ. Closed curves are included in this formalism by the convention that $\partial\Gamma = \emptyset$ for them. We call $H^{1/2}(\Gamma)$ the trace Sobolev–Slobodeckij space, which is endowed with the Slobodeckij norm (see, e.g., [32] or [33]):

$$\|w\|^2_{1/2,\Gamma} := \|w\|^2_{0,\Gamma} + \int_\Gamma \int_\Gamma \frac{|w(x) - w(y)|^2}{|x - y|^2} dxdy \tag{6}$$

For open curves, $H_{00}^{1/2}(\Gamma) \subset H^{1/2}(\Gamma)$ is introduced as the subspace of functions, which can be extended by 0 as they approach the extremity points $\partial\Gamma$. It is endowed with the norm (see, e.g., [32], Section 1.1)

$$\|w\|_{H_{00}^{1/2}(\Gamma)} := \|w\|^2_{1/2,\Gamma} + \int_\Gamma \frac{1}{\operatorname{dist}(x, \partial\Gamma)} |w(x)|^2 dx \tag{7}$$

For closed curves, we set the convention $H_{00}^{1/2}(\Gamma) := H^{1/2}(\Gamma)$. For any $v \in V$, owing to the fact that $[v]|_{\partial\Gamma} = 0$, we have $[v] \in H_{00}^{1/2}(\Gamma)$. Let $\boldsymbol{\lambda} := \boldsymbol{\sigma} \cdot \boldsymbol{n}$ be the surface force that Ω_2 applies to Ω_1 at the interface. Its components then belong to $H^{-1/2}(\Gamma)$, which is the topological dual space of $H_{00}^{1/2}(\Gamma)$, thus equipped with the operator norm

$$\|\lambda\|_{-1/2,\Gamma} := \sup_{w \in H_{00}^{1/2}(\Gamma)} \frac{\int_\Gamma \lambda w ds}{\|w\|_{H_{00}^{1/2}(\Gamma)}} \tag{8}$$

We then have an equivalence of norms, in the sense that for any $v \in V$, $\|[v]\|_{H_{00}^{1/2}(\Gamma)} \leqslant C\|v\|_{1,\Omega_1 \cap \Omega_2}$ and for any $w \in H_{00}^{1/2}(\Gamma)$, there exists a $v \in V$ such that $[v] = w$ and $\|v\|_{1,\Omega_1 \cap \Omega_2} \leqslant C\|w\|_{H_{00}^{1/2}(\Gamma)}$ (see [34], Appendix A). In this way, an equivalent definition of $H^{-1/2}$ norm is

$$\|\lambda\|_{-1/2,\Gamma} := \sup_{w \in V} \frac{\int_\Gamma \lambda [w] ds}{\|w\|_{1,\Omega_1 \cup \Omega_2}} \tag{9}$$

To obtain (9) while releasing the assumption that $[v]|_{\partial\Gamma} = 0$, Appendix A of [34] may be consulted. To give problems (1–5), a weak formulation, bilinear and linear forms are, respectively, defined as

$$\text{For } (\boldsymbol{u}, \boldsymbol{v}) \in V^2 \times V^2, a(\boldsymbol{u}, \boldsymbol{v}) := \sum_{i=1}^{2} \int_{\Omega_i} \boldsymbol{\sigma}(\boldsymbol{u}_i) : \boldsymbol{\epsilon}(\boldsymbol{v}_i) dx \tag{10}$$

$$\text{For } \boldsymbol{v} \in V^2, l(\boldsymbol{v}) := \sum_{i=1}^{2} \int_{\Omega_i} \boldsymbol{f}_i \cdot \boldsymbol{v}_i dx + \int_{\Gamma_g^i} \boldsymbol{g}_i \cdot \boldsymbol{v}_i ds \tag{11}$$

Denoting $M := H^{-1/2}(\Gamma)$, an additional bilinear form is introduced, which will be useful to enforce constraint (4)

$$\text{For } \boldsymbol{v} \in V^2 \text{ and } \boldsymbol{\mu} \in M^2, b(\boldsymbol{v}, \boldsymbol{\mu}) := \int_{\Gamma} [\boldsymbol{u}] \cdot \boldsymbol{\mu} ds \tag{12}$$

The weak formulation of the problem then reads, find $\boldsymbol{u} \in V^2, \boldsymbol{\lambda} \in M^2$ such that

$$\forall \boldsymbol{v} \in V^2, a(\boldsymbol{u}, \boldsymbol{v}) + b(\boldsymbol{v}, \boldsymbol{\lambda}) = l(\boldsymbol{v}) \tag{13}$$

$$\forall \boldsymbol{\mu} \in M^2, b(\boldsymbol{u}, \boldsymbol{\mu}) = 0 \tag{14}$$

For the sake of conciseness, we shall in the mathematical developments of this paper rather work with a *scalar* second-order elliptic problem—this corresponds to a heat diffusion problem in a bimaterial. All theorems will be presented in their scalar version, but their vectorized counterparts could be derived in a similar way. Bilinear form $a \in \mathcal{L}(V, V)$ and $b \in \mathcal{L}(V, M)$ are then

$$a(u, v) := \sum_{i=1}^{2} \int_{\Omega_i} (\boldsymbol{A}_i \cdot \nabla u_i) \cdot \nabla v_i dx \tag{15}$$

$$b(v, \mu) := \int_{\Gamma} [u] \mu ds \tag{16}$$

where $\boldsymbol{A}_i$ is the second-order tensor of conductivity. Linear form $l \in \mathcal{L}(V)$ is

$$l(v) := \sum_{i=1}^{2} \int_{\Omega_i} f_i v_i dx \tag{17}$$

The multiplier $\lambda := (\boldsymbol{A} \cdot \nabla u) \cdot \boldsymbol{n}$ then corresponds to the normal heat flux on the interface.

3. DISCRETIZATION OF PRIMAL AND DUAL SPACES

In this first phase, we focus exclusively on the use of Lagrange multipliers. So the interface is assumed to be straight for now and thus exactly described. We suppose that Ω is meshed with a family $\mathcal{T}_h$ of *affine* triangular meshes, which is assumed to be quasi-uniform and regular: for $K \in \mathcal{T}_h$, denoting h_K as the radius of the smallest circle containing K and ρ_K as the radius of the largest circle containing K, and setting the characteristic mesh size to $h := \max_K h_K$, we have

Assumption (H1). There exists a constant C independent of h and K such that $\frac{h}{\rho_K} \leqslant C$. The angles of triangle K are consequently uniformly bounded away from 0.

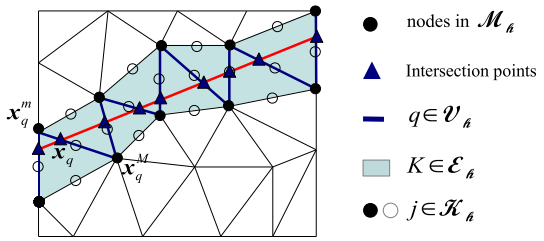

Figure 2. Some topological definitions around the interface.

3.1. Discretization of the field of unknowns

We call $\mathcal{E}_h$ the set of elements of $\mathcal{T}_h$ cut by Γ and $\mathcal{V}_h$ the corresponding intersected edges. Let $\mathcal{N}_h \subset \mathbb{N}$ be the nodes of the mesh, each node being identified by a number. Nodes of elements in $\mathcal{E}_h$ will be denoted $\mathcal{K}_h \subset \mathcal{N}_h$ and the subset of *vertex* nodes by $\mathcal{M}_h \subset \mathcal{K}_h$ (see Figure 2). For an intersected edge $q \in \mathcal{V}_h$, $\boldsymbol{x}_q$ represents the position of the associated intersection point. Moreover, we denote $q_m \in \mathcal{M}_h$ and $q_M \in \mathcal{M}_h$ the nearest and farthest connected vertex nodes, respectively, and $\boldsymbol{x}_q^m, \boldsymbol{x}_q^M$ their positions (see Figure 2).

Classically, the discrete field space is then (see [1])

$$V_h := \left\{ \sum_{i \in \mathcal{N}_h} a_i N_i(\boldsymbol{x}) + \sum_{j \in \mathcal{K}_h} b_j N_j(\boldsymbol{x}) H(\boldsymbol{x}), a_i \in \mathbb{R}, b_i \in \mathbb{R} \right\} \tag{18}$$

where H is the Heaviside-like function used to represent the jump:

$$H(\boldsymbol{x}) = \begin{cases} -1 \text{if } \boldsymbol{x} \in \Omega_1 \\ 1 \text{if } \boldsymbol{x} \in \Omega_2 \end{cases} \tag{19}$$

3.2. Discretization of the multipliers

For the approximation to be independent of the crack location, the multiplier components are defined on the parent nodes $\mathcal{M}_h$, as in [17, 18, 24]. Then

$$\bar{M}_h := \left\{ \boldsymbol{x} \in \mathcal{E}_h \to \sum_{i \in \mathcal{M}_h} \mu_i N_i^{\text{lin}}(\boldsymbol{x}), \mu_i \in \mathbb{R} \right\} \tag{20}$$

where N_i^{lin} is the *linear* shape function associated with *vertex* node i. The approximation space M_h for the multipliers is then

$$M_h = \left\{ \mu \mid_\Gamma, \mu \in \bar{M}_h \right\} \tag{21}$$

As mentioned in the Introduction, the interpolation of the pressure multipliers should additionally abide by a so-called discrete inf-sup condition to yield stable results (see [16, 18])

$$\exists c > 0 \text{ independent of h}, \ \forall \mu_h \in M_h, \ \sup_{v_h \in \boldsymbol{V}_h} \frac{\int_\Gamma \mu_h [v_h] d\Gamma}{\|v_h\|_{1,\Omega_1 \cup \Omega_2}} \geqslant c h^{1/2} \|\mu_h\|_{0,\Gamma} \tag{22}$$

This condition basically states that the discrete multiplier space should not be too rich in comparison with the discrete displacement one. Otherwise, spurious oscillations of the pressure multipliers are observed (see [12]). Hence, equality relations have to be prescribed between some multiplier components on $\mathcal{M}_h$, thus reducing $\bar{M}_h$, as in [17, 18]. Two restriction algorithms have been considered (the first from [18], and the second is newly proposed):

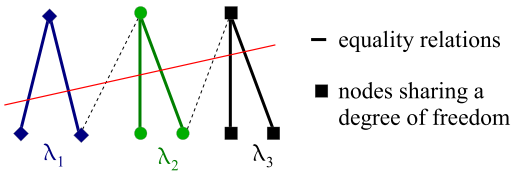

Figure 3. Restriction algorithm $P1^{-}$, as defined by Béchet and al [18].

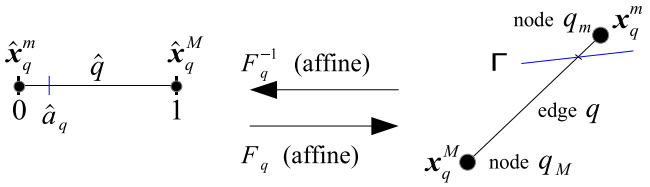

Figure 4. Closely intersected edge.

(1) The algorithm of [18] with continuous piecewise linear or constant multipliers that we will denote by the acronym $P1^{-}$. It is illustrated on Figure 3 and is intended to be used along with a linear interpolation of the displacement. Such a formulation will be denoted by $P1/P1^{-}$;
(2) A new algorithm of P1 multipliers with less constraints referred to as $P1^{*}$ from here onward. It verifies $P1^{-} \subset P1^{*}$ and is intended for a combined use along with a piecewise quadratic displacement and will be called $P2/P1^{*}$.

*3.3. Design of multiplier space P1**

As a higher-order interpolation of the displacement makes a given pressure interpolation more likely to satisfy the inf-sup condition, the idea behind the construction of algorithm $(P1^{*})$ was to release some constraints from $(P1^{-})$. Let us set a parameter $\kappa \ll 1$ and introduce the following preliminary definitions:

Definition 3.1
Closely intersected edge. Let $q \in \mathcal{V}_h$ be an intersected edge. It is mapped onto a reference segment $\hat{q}$ with an affine map, in such a way that q_m be mapped onto 0, so that the reference coordinate $\hat{a}_q$ of the intersection point verifies $\hat{a}_q \leqslant 1/2$, as shown in Figure 4. The edge is called closely intersected if $\hat{a}_q \leqslant \kappa$.
Almost coincident node. $n \in \mathcal{M}_h$ is an almost coincident node if there exists a closely intersected edge $q \in \mathcal{V}_h$ such that $n = q_m$.

Definition 3.2
Slanted triangle. Let us consider any $K \in \mathcal{E}_h$. Two of its edges are intersected and the subcell containing their common node is called *triangular subcell*. This common node is mapped onto the origin of the reference triangle $\hat{K}$ (see Figure 5). Such a map is moreover chosen such that the first reference coordinate corresponds to the largest coordinate $\hat{a}_M$ among the intersection points, whereas the second reference coordinate is associated with the smallest $\hat{a}_m$ (see Figure 5). We then call *slanted* a triangle with an « elongated » triangular subcell, such that $\frac{\hat{a}_m}{\hat{a}_M} \leqslant \kappa$.

Asymptotically speaking, we should rather call *slanted* family of meshes, for which ratio $\frac{\hat{a}_m}{\hat{a}_M}$ decreases with mesh refinement and is not bounded away from zero as $h \to 0$.

Algorithm $P1^{*}$ will be built so as to prevent some basic flaws—high conditioning and redundancy—in the first stage and in the second stage, we will analytically prove that the resulting construction is actually sufficient to pass the inf-sup condition.

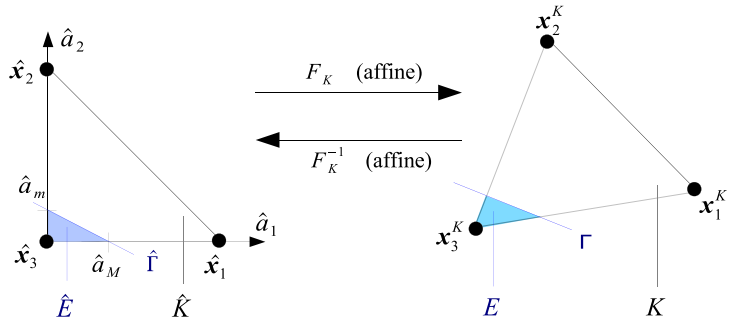

Figure 5. Intersected triangle.

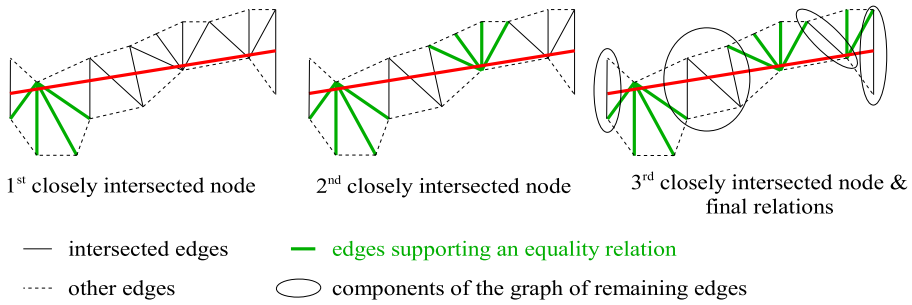

Figure 6. Building algorithm P1* with closely intersected edges.

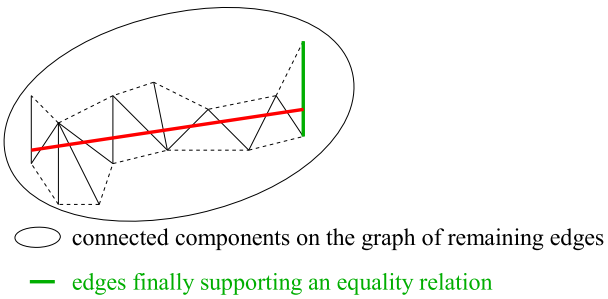

Figure 7. Minimal restriction algorithm without closely intersected edges.

Definition 3.3
Restricted multiplier space $P1^*$ defining M_h. The minimal restriction algorithm is as follows:

(1) Initialization of a working set of edges $\mathcal{C}_h = \mathcal{V}_h$.
(2) For each almost coincident node n, for each closely intersected edge q emanating from n (i.e., $n = q_m$), an equality relation is assigned linking n to the opposite vertex q_M, provided q_M is not already involved in another relation.
(3) All edges thus supporting an equality relation are removed from $\mathcal{C}_h$.
(4) Components of $\mathcal{C}_h$, in the sense of the graph theory, are listed.
(5) For each such component, if a vertex is already linked, no additional equality relation is assigned (see Figure 6). If not, a single additional equality relation is assigned for the whole component (see Figure 7), so as to preclude redundant combinations, as explained in Theorem 3.1.

Figures 6 and 7 provide examples of this algorithm with and without almost coincident nodes. Note that no further relation is needed after dealing with almost coincident nodes on Figure 6.

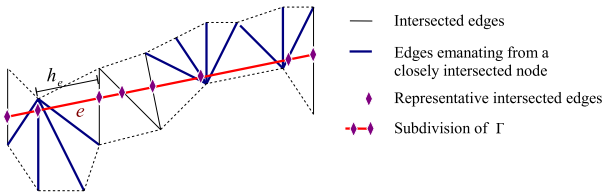

Figure 8. Subdivision of the interface.

3.4. Non-redundancy

Any well-defined algorithm restriction requires the linear independence of the traces on Γ of the functions in $\bar{M}_h$, otherwise, the problem becomes singular. Singular combinations could be detected through the computation of the kernel of the mass matrix $\int_\Gamma N_k^{\text{lin}} N_l^{\text{lin}} d\Gamma$, as seen in [24]. Here, aiming at a topological construction of M_h, we will rather show that

Theorem 3.1
Let $\mu_h \in \bar{M}_h$, if $\mu_h|_\Gamma = 0$ then $\mu_h = 0$.

Proof
For L a Lagrange DOF and $\mathcal{L} \subset \mathcal{M}_h$ the set of nodes sharing it, we set $\psi_L := \sum_{l \in \mathcal{L}} N_l^{\text{lin}}$. Let us suppose a combination $\mu_h = \sum_L \mu_L \psi_L$ having zero trace. The sum can be split into the connected components of the graph of $\mathcal{V}_h$. For each component, after the minimal restriction algorithm defining $P1^*$, there exists an edge q supporting an equality relation. Because $\mu_q := \mu_h(\boldsymbol{x}_q) = 0, \mu_h\left(\boldsymbol{x}_q^m\right) = \mu_h\left(\boldsymbol{x}_q^M\right) = 0$. It follows that for an edge q' emanating from q_m or q_M because $\mu_{q'} = 0$, we have $\mu_h\left(\boldsymbol{x}_{q'}^m\right) = \mu_h\left(\boldsymbol{x}_{q'}^M\right) = 0$. The coefficients are shown to be zero on all nodes of the connected component repeating the procedure iteratively. In other terms, we have proven that for each connected component of the graph, without restriction algorithm, there would be exactly one degenerate mode, which corresponds to the case where the multiplier components are proportional to the signed distance to the interface. □

3.5. Proof of the discrete inf-sup condition

We are now able to prove the inf-sup condition analytically

Theorem 1
Assume Γ to be a straight line and assume that none of the intersected triangle is slanted. Then, discretization $(P2/P1^*)$ fulfills the discrete inf-sup condition (22).

Proof Step 1. As in [18], a subdivision of Γ is introduced for the sake of the proof: a single representative edge is selected among closely intersected edges emanating from a common almost coincident node, whereas non-closely intersected edges are all selected. Segments e with length h_e between the thus selected intersection points make a subdivision for Γ (see Figure 8).

Let $\mu_h \in M_h$. We define mesh-dependent norms as $\|\mu_h\|^2_{-1/2,\Gamma h} := \sum_{e \in \Gamma} h_e \|\mu_h\|^2_{0,e}$ and $\|\mu_h\|^2_{1/2,\Gamma h} := \sum_{e \in \Gamma} \frac{1}{h_e} \|\mu_h\|^2_{0,e}$.

Step 2. Let us prove the existence of c, C such that $ch \leqslant h_e \leqslant Ch$. Let e be an element of the subdivision, and K be the triangle such that $e \cap K \neq \emptyset$ and such that $\hat{\lambda}_M > \kappa$ (see Figure 9): *reductio ad absurdum*, it is obvious that such a triangle exists after the definition of the subdivision.

Then $h_e \geqslant \hat{a}_M |\boldsymbol{x}_1 - \boldsymbol{x}_3| \sin(\theta_K) \geqslant 2\rho_K \kappa \sin(\theta_K)$ (see Figure 9). As stated previously, regularity assumption (H1) ensures that θ_K is uniformly bounded away from zero, which implies that $h_e \geqslant ch$. This also implies that a limited number N of triangles may

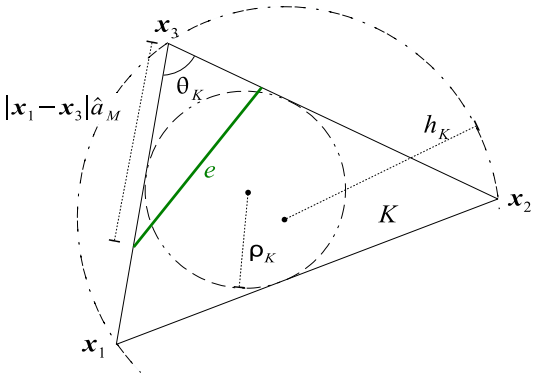

Figure 9. Intersected element K.

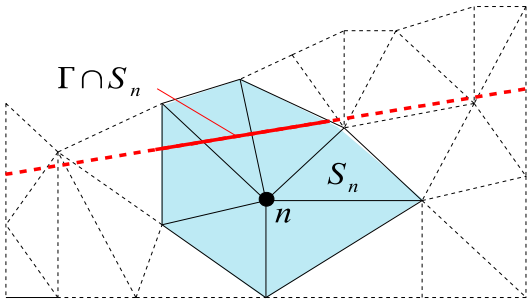

Figure 10. Support of node n.

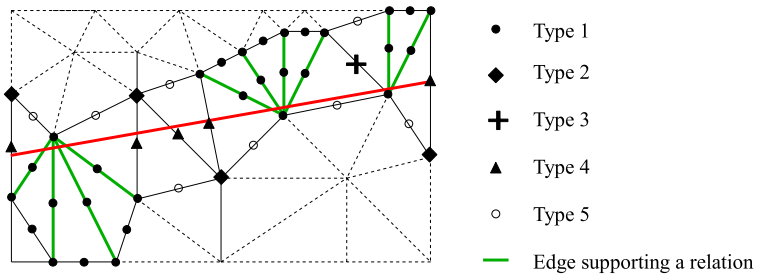

Figure 11. Nodes classification.

be crossed by element e, hence, $h_e \leqslant 2Nh$. An immediate consequence is that norms $\|.\|_{-1/2,\Gamma h}$ and $h^{1/2}\|.\|_{0,\Gamma}$ are equivalent.

Step 3. As has been done in [18], we look for $v_h \in V_h$ such that $[v_h] = \mu_h$, which give the displacement approximation (18) amounts to seeking the enriched DOF b_n such that

$$\mu_h = 2 \sum_{n \in \mathcal{K}_h} b_n N_n|_\Gamma \tag{23}$$

and such that those coefficients be uniformly bounded by the neighboring pressure

$$\exists C,\ \forall n,\ |b_n| \leqslant C\,|\mu_h|_{0,\infty,\Gamma\cap S_n} \tag{24}$$

where S_n denotes the support of n (see Figure .10).

Let us classify the nodes in $\mathcal{K}_h$ (see Figure 11):

- Type 1. n is located on an edge supporting an equality relation or is a node located exactly on the interface.
- Type 2. n is a non-type 1 vertex node.

- Type 3. n is a non-type 1 middle node, whose associated edge is intersected and both ends of which are subjected to equality relations.
- Type 4. n is a non-type 3 middle node on an intersected edge.
- Type 5. n is a middle node on a non-intersected edge.

Coefficients b_n were chosen such that

- Type 1. Node n belongs to an edge q supporting an equality relation. We denote L the Lagrange DOF thus shared by the whole edge. We have $\mu_q = \mu_L$. Let us set $b_n = \mu_L/2$, it implies $[u](\boldsymbol{x}_q) = \mu_q$ and (24) holds.
- Type 2. We set $b_n = 0$.
- Type 3. Let q be the intersected edge n belongs to (see Figure 12). Let K and L be the $\bar{M}_h$ DOFs, and q_M and q_m are associated (see Figure 12). We set $b_n = \frac{\mu_K+\mu_L}{4}$, which obviously abides by (24). Given that $\mu_q = \left(1-\hat{a}_q\right)\mu_L + \hat{a}_q\mu_K$, we may check that $[u](\boldsymbol{x}_q) = 2\sum_{l\in\{n,q_M,q_m\}} b_l N_l\left(\hat{a}_q\right) = \mu_q$.
- Type 4: Once again, q denotes the intersected edge n belongs to. b_n is then taken as $2b_n = \frac{1}{N_n(\hat{a}_q)}\left(\mu_q - 2\sum_{l\in\{q_M,q_m\}} b_l N_l\left(\hat{a}_q\right)\right)$. An easy calculation then yields $[u](\boldsymbol{x}_q) = \mu_q$. We know that q is not closely intersected (otherwise, n would be a type 1 or 3). As a result, it holds $\hat{a}_q \geqslant \kappa$ and $N_n\left(\hat{a}_q\right) \geqslant 4\kappa(1-\kappa)$ because $\hat{a}_q \leqslant 1/2$. Any vertex nodes at the end of q is either a type 2, in which case it bears a zero as enriched DOF, or a type 1, in which case it bears a M_h DOF μ_L. It implies (24) because $2|b_n| \leqslant \frac{1}{2\kappa(1-\kappa)}\max\{\mu_q,\mu_L\} \leqslant \frac{1}{2\kappa(1-\kappa)}|\mu_h|_{0,\infty,\Gamma\cap S_n}$.
- Type 5: At this stage, the displacement jump is equal to μ_h on all intersection points. So the remaining work to obtain (23) consists in making this jump linear in between. Let $K \in \mathcal{E}_h$ be the intersected triangle n belongs to (see Figure 13). Denoting $e := \Gamma \cap K$, we propose some evidence that can be found b_n such that

$$\sum_{l\in\mathcal{K}_h\cap K} b_l N_l|_e \in P_1(e) \tag{25}$$

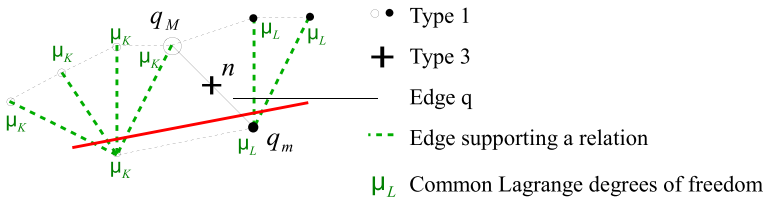

Figure 12. Node of type 3.

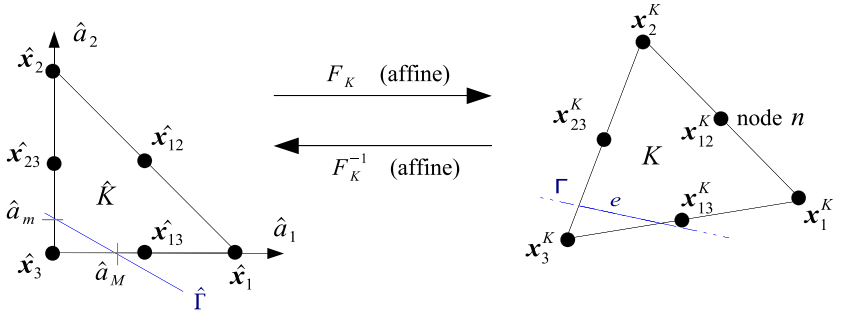

Figure 13. Cut element K.

As the interface is straight and the mapping affine, e is described by $e : \hat{a}_2 - \hat{a}_m + \frac{\hat{a}_m}{\hat{a}_M}\hat{a}_1 = 0$ (see Figure 13). Therefore, we may rewrite

$$\sum_{l\in\mathcal{K}_h\cap K} b_l N_l|_e = \sum_{l\in\mathcal{K}_h\cap K} b_l N_l\left(\hat{a}_1, \hat{a}_m\left[1 - \frac{\hat{a}_1}{\hat{a}_M}\right]\right) \tag{26}$$

This expression is a second-order polynomial of $\hat{a}_1$ and as such is linear if and only if the second-order coefficient is zero. Calling b_i^K the enriched DOF of the node located at $\boldsymbol{x}_i^K$ (see Figure 13) and replacing the shape functions by their expressions, the corresponding equation turns into

$$b_n = b_{12}^K = \frac{b_1^K + r^2 b_2^K + (1-r)^2 b_3^K + 2r(1-r)b_{23}^K - 2(1-r)b_{13}^K}{2r} \tag{27}$$

where $r := \hat{a}_m/\hat{a}_M$ verifies $0 < \kappa \leqslant r \leqslant 1$ because slanted triangles have been excluded. It follows that $|b_n| \leqslant \frac{3}{\kappa} \max_{i\in\{1,2,3,23,13\}} \left|b_i^K\right| \leqslant C|\mu_h|_{0,\infty,\Gamma\cap S_n}$ so (24) holds.

The displacement thus generated verifies (24). Because it coincides with the pressure at the intersection points and is piecewise linear in between, (23) holds. The demonstration follows [18] from now on. It is briefly recalled for the sake of self-sufficiency.

Step 4. Prove that $\|\mu_h\|_{-1/2,\Gamma h}\|[w_h]\|_{1/2,\Gamma h} \leqslant C\int_\Gamma \mu_h[w_h]d\Gamma$.
Because $[w_h] = \mu_h|_\Gamma$, we have $\int_\Gamma \mu_h[w_h]ds = \|\mu_h\|_{0,\Gamma}^2$. This implies that $\|\mu_h\|_{-1/2,\Gamma h}\|[w_h]\|_{1/2,\Gamma h} = \left(\sum_{e,e'} \frac{h_e}{h_{e'}}\|\mu_h\|_{0,e}^2\|\mu_h\|_{0,e'}^2\right)^{1/2}$. Because $\frac{h_e}{h_e'}$ is bounded, as proven in Step 2, it may be concluded that $\|\mu_h\|_{-1/2,\Gamma h}\|[w_h]\|_{1/2,\Gamma h} \leqslant C\|\mu_h\|_{0,\Gamma}^2 = C\int_\Gamma \mu_h[w_h]d\Gamma$.

Step 5. Prove that $\sum_{q\in\mathcal{V}_h} \mu_q^2 \leqslant C\|[w_h]\|_{1/2,\Gamma h}^2$.
Using the pullback onto the reference unit segment $\hat{e}$ for the mesh-dependent norms, it holds $\|\mu_h\|_{1/2,\Gamma h}^2 = \sum_e h_e^{-1}\|\mu_h\|_{0,e}^2 = \sum_e \|\hat{\mu}_h\|_{0,\hat{e}}^2$. The equivalence of all norms on the finite dimensional space of linear functions on $\hat{e}$ yields $\|\mu_h\|_{0,\infty,e} = \|\mu_h\|_{0,\infty,\hat{e}} \leqslant C\,\|\hat{\mu}_h\|_{0,\hat{e}}$. Moreover, an element e crosses a limited number of edges, given the regularity of the mesh, as pointed out in Step 2, so that $\sum_{q\in\mathcal{V}_h} \mu_q^2 \leqslant C\sum_e \|\mu_h\|_{0,\infty,e}^2$, which gives the result because $[w_h] = \mu_h|_\Gamma$.

Step 6. Prove that $\|w_h\|_{1,\Omega_1\cup\Omega_2}^2 \leqslant C\sum_{q\in\mathcal{V}_h} \mu_q^2$.
It can easily be shown with a transformation onto the reference triangle that $\|w_h\|_{0,M}^2 \leqslant Ch^2 \sum_{K\in\mathcal{T}_h} \|\hat{w}_h\|_{0,\hat{K}}^2$. Because $\|\hat{w}_h\|_{0,\hat{K}}^2 \leqslant 4\sum_{i=1..6} b_i^2\|N_i\|_{0,\hat{K}}^2$ and the triangulation is regular, we may assert that $\|w_h\|_{0,\Omega}^2 \leqslant Ch^2\sum_{n\in\mathcal{K}_h} b_n^2$. An inverse approximation yields $\|w_h\|_{1,\Omega_1\cup\Omega_2} \leqslant Ch^{-1}\|w_h\|_{0,\Omega}$, so $\|w_h\|_{1,\Omega_1\cup\Omega_2}^2 \leqslant C\sum_{n\in\mathcal{K}_h} b_n^2$. Using Step 3, this implies that $\|w_h\|_{1,\Omega_1\cup\Omega_2}^2 \leqslant C\sum_{n\in\mathcal{K}_h} \|\mu_h\|_{0,\infty,\Gamma\cap S^n}^2$. Each intersected edge belongs to a limited number of supports S_n (with quadratic triangles, 9 is an upper bound for a shared edge), so $\sum_{n\in\mathcal{K}_h} \|\mu_h\|_{0,\infty,\Gamma\cap S_n}^2 \leqslant 9\sum_{q\in\mathcal{V}_h} \mu_q^2$, which yields the result.

Step 7. Conclusion.
Steps 5 and 6 yield $\|w_h\|_{1,\Omega_1\cup\Omega_2} \leqslant C\|[w_h]\|_{1/2,\Gamma h}$. Hence, we may assert that

$$\sup_{v_h \in \boldsymbol{V}_h} \frac{\int_\Gamma \mu_h [v_h] d\Gamma}{\|v_h\|_{1,\Omega_1 \cup \Omega_2}} \geqslant \frac{\int_\Gamma \mu_h [w_h] d\Gamma}{\|w_h\|_{1,\Omega_1 \cup \Omega_2}} \geqslant c \frac{\int_\Gamma \mu_h [w_h] d\Gamma}{\|[w_h]\|_{1/2,\Gamma_h}} \tag{28}$$

And because of Step 4, $\frac{\int_\Gamma \mu_h [w_h] d\Gamma}{\|[w_h]\|_{1/2,\Gamma_h}} \geqslant c\|\mu_h\|_{-1/2,\Gamma h}$. With the equivalence proven in Step 2 between $\|.\|_{-1/2,\Gamma h}$ and $h^{1/2}\|.\|_{0,\Gamma}$, we finally have $\frac{\int_\Gamma \mu_h [w_h] d\Gamma}{\|w_h\|_{1,\Omega_1 \cup \Omega_2}} \geqslant c h^{1/2} \|\mu_h\|_{0,\Gamma}$. □

3.6. Interpolation properties of the discrete multiplier spaces

An important point to the error analysis is to estimate the ability of the discrete multiplier spaces to approach a continuous function. Hence, we shall define an interpolant π_h of λ onto M_h

Definition 3.4
For L as a DOF of the reduced space M_h, ψ_L its shape function, and S_L the support of ψ_L, we set $\lambda_L := \frac{\int_\Gamma \lambda \psi_L d\Gamma}{\int_\Gamma \psi_L d\Gamma} = \frac{\int_{\Gamma \cap S_L} \lambda \psi_L d\Gamma}{\int_{\Gamma \cap S_L} \psi_L d\Gamma}$. Taking a cue on the quasi-interpolation operators of Clément [35], we build $\pi_h \lambda$ as $\pi_h \bar{\lambda} := \sum_L \lambda_L \psi_L$, which may as well be regarded as an element of $\bar{M}_h$.

Let us start with stability properties for π_h

Lemma 3.1
Operator π_h is H^1-stable and L^2-stable, that is to say, $\|\pi_h \lambda\|_{1,\Gamma} \leqslant C\|\lambda\|_{1,\Gamma}$ and $\|\pi_h \lambda\|_{0,\Gamma} \leqslant C\|\lambda\|_{0,\Gamma}$. Moreover, $|\pi_h \lambda|^2_{1,\mathcal{E}_h} \leqslant Ch|\lambda|^2_{1,\Gamma}$.

Proof
We have $\|\pi_h \lambda\|^2_{0,\Gamma} \leqslant \sum_L \lambda_L^2 \|\psi_L\|^2_{0,\Gamma}$. Because $\psi_L \geqslant 0$, applying Schwarz inequality to the definition of λ_L gives $\lambda_L^2 \leqslant \frac{\|\lambda\|^2_{0,\Gamma \cap S_L}}{\|\psi_L\|^2_{1,0,\Gamma}} \|\psi_L\|^2_{0,\Gamma}$. Shape function ψ_L verifies $\|\psi_L\|_{0,\Gamma} \leqslant Ch^{\frac{1}{2}}$ and the inverse property $\|\psi_L\|_{0,\Gamma} \leqslant Ch^{-\frac{1}{2}} \|\psi_L\|_{0,1,\Gamma}$, hence, $\|\pi_h \lambda\|^2_{0,\Gamma} \leqslant C \sum_L \|\lambda\|^2_{0,\Gamma \cap S_L} \leqslant C\|\lambda\|^2_{0,\Gamma}$ so the operator is L^2 stable.

As for the H^1 stability, on a support S_L, let us call I and the adjacent DOFs. Because $\psi_I + \psi_J + {}_L = 1$ over S_L, we have $\nabla(\pi_h \lambda) = (\lambda_J - \lambda_I)\nabla\psi_J + (\lambda_L - \lambda_I)\nabla\psi_L$ so that

$$|\pi_h \lambda|^2_{1,S_L \cap \Gamma} \leqslant Ch^{-1} |\lambda_J - \lambda_I|^2 \tag{29}$$

Let $F := h\,Id$ be a « dilatation » mapping from an adimensional reference space onto the real one. Let $\hat{\psi} := \quad \circ F, \hat{\lambda} := \lambda \circ F, \hat{\Gamma} := F^{-1}(\Gamma)$ and $\hat{S}_L := F^{-1}(S_L)$. An equivalent definition for λ_L is then $\lambda_L := \frac{\int_{\hat{\Gamma} \cap \hat{S}_L} \hat{\lambda} \hat{\psi}_L d\Gamma}{\int_{\hat{\Gamma} \cap \hat{S}_L} \hat{\psi}_L d\Gamma}$. With this definition, we introduce the linear form $\hat{l}\left(\hat{\lambda}\right) = \lambda_L - \lambda_I$. Schwarz inequality and the equivalence of all norms for $\hat{\psi}_L$ yield $\left|\hat{l}\left(\hat{\lambda}\right)\right| \leqslant C \left\|\hat{\lambda}\right\|_{0,\hat{S}_L \cap \hat{\Gamma}} \leqslant C \left\|\hat{\lambda}\right\|_{1,\hat{S}_L \cap \hat{\Gamma}}$, hence, $\hat{l}$ is continuous and vanishes for constants, so we may apply Bramble–Hilbert lemma ([36], Theorem 4.1.3): $\left|\hat{l}\left(\hat{\lambda}\right)\right| \leqslant C \left|\hat{\lambda}\right|_{1,\hat{S}_L \cap \hat{\Gamma}}$. Pulling the right-side member onto the real space, we have $\left|\hat{l}\left(\hat{\lambda}\right)\right|^2 \leqslant Ch|\lambda|^2_{1,S_L \cap \Gamma}$, which is given in (29) that yields $|\pi_h \lambda|^2_{1,K \cap \Gamma} \leqslant C|\lambda|^2_{1,S_L \cap \Gamma}$. Summing up over the intersected elements yields $|\pi_h \lambda|^2_{1,\Gamma} \leqslant C|\lambda|^2_{1,\Gamma}$. Replacing (29) with $|\pi_h \lambda|^2_{1,K} \leqslant C|\lambda_J - \lambda_I|^2$, it comes $|\pi_h \lambda|^2_{1,\mathcal{E}_h} \leqslant Ch|\lambda|^2_{1,\Gamma}$. □

Let us now determine common interpolation properties to $P1^*$ and $P1^-$ as follows.

Lemma 3.2
For multiplier spaces $P1^*$ and $P1^-$, it holds

$$\forall \lambda \in H^1(\Gamma), \|\pi_h \lambda - \lambda\|_{0,\Gamma} \leqslant Ch\,\|\lambda\|_{1,\Gamma} \tag{30}$$

and

$$\forall \lambda \in H^{1/2}(\Gamma), \|\pi_h \lambda - \lambda\|_{0,\Gamma} \leqslant C h^{1/2} \|\lambda\|_{1/2,\Gamma} \tag{31}$$

Proof
Adopting similar definitions as in the proof of Lemma 3.1, over $\hat{S}_L$, it reads $\pi_h \hat{\lambda} = \lambda_L + (\lambda_J - \lambda_L)\hat{\psi}_J + (\lambda_I - \lambda_L)\hat{\psi}_I$. Then, we have $\left\|\pi_h \hat{\lambda} - \hat{\lambda}\right\|_{0,\hat{\Gamma}\cap\hat{S}_L} \leqslant \left\|\lambda_L - \hat{\lambda}\right\|_{0,\hat{\Gamma}\cap\hat{S}_L} + |\lambda_I - \lambda_L| \left\|\hat{\psi}_I\right\|_{0,\hat{\Gamma}\cap\hat{S}_L} + |\lambda_J - \lambda_L| \left\|\hat{\psi}_J\right\|_{0,\hat{\Gamma}\cap\hat{S}_L}$. From Poincaré–Wirtinger inequality (see [37], Corollary 5.4.1 and its proof), it comes $\left\|\lambda_L - \hat{\lambda}\right\|_{0,\hat{\Gamma}\cap\hat{S}_L} \leqslant C \left|\hat{\lambda}\right|_{1,\hat{\Gamma}\cap\hat{S}_L}$. Because $\left\|\hat{\psi}_I\right\|_{0,\hat{\Gamma}\cap\hat{S}_L}$ is bounded, and $|\lambda_I - \lambda_L| \leqslant C \left|\hat{\lambda}\right|_{1,\hat{\Gamma}\cap\hat{S}_L}$ after the proof of Lemma 3.1, it becomes $\left\|\pi_h \hat{\lambda} - \hat{\lambda}\right\|_{0,\hat{\Gamma}\cap\hat{S}_L} \leqslant C \left|\hat{\lambda}\right|_{1,\hat{\Gamma}\cap\hat{S}_L}$, pulling this result onto the physical space and summing up over L yields (30). As for (31), it follows from (30) and Lemma 3.1 appealing to the interpolation theory: the argument is rather technical and classically used for quasi-interpolation operators (see for instance Chen and Nochetto [38], Lemma 3.2). □

Establishing an improved accuracy for $P1^*$ would imply to improve (30) by using vanishing operators for all *affine* functions. In fact, this would solely be possible if the interface cuts the mesh *far from nodes*, otherwise, the multiplier stays piecewise constant on small intersections of the mesh and the interface. Nevertheless, to have some understanding of this case without going too far into technicalities, let us consider a nodal interpolation operator instead of π_h. In this simplified analysis, it is assumed that meas$(\Gamma) = 1$ and that it is uniformly subdivided into segments of length h (see Figure 14). If $a \in [0, 1]$ is the extremity of such a segment, let us assume that λ and $\pi_h\lambda$ coincide at a and $a + h$. In the case where a corresponds to an almost coincident node, $\pi_h\lambda$ is taken to be constant on $[a, a + \kappa h]$ and linear on $[a + \kappa h, a + h]$ (see Figure 14). Otherwise, $\pi_h\lambda$ is linear on $[a, a + h]$ (see Figure 14).

In the first case (almost coincident node), some trapezoid rule analogous L^1 error estimate yields

$$\|\lambda - \pi_h\lambda\|_{0,1,[a,a+h]} \leqslant h^2 \frac{\kappa}{2} |\lambda|_{1,\infty,\Gamma} + \frac{h^3}{12} |\lambda|_{2,\infty,\Gamma} \tag{32}$$

We recall that κ represents the intersection ratio under which an edge is considered closely intersected, which implies the imposition of some equality relations making the P0-segment to appear. Assuming a random configuration of intersection—which should happen if the mesh is built regardless of the interface—such P0-segments embedding elements therefore occur with a probability κ on Γ. The rest of them are fully P1. Therefore, an L^1 error estimate is

$$\|\lambda - \pi_h\lambda\|_{0,1,\Gamma} \leqslant h \frac{\kappa^2}{2} |\lambda|_{1,\infty,\Gamma} + \frac{h^2}{12} |\lambda|_{2,\infty,\Gamma} \tag{33}$$

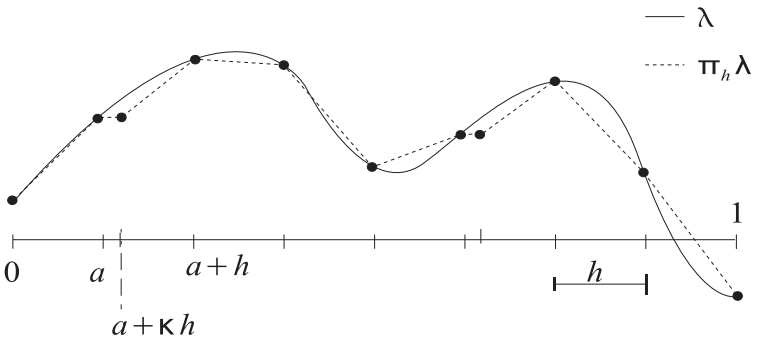

Figure 14. Illustration of the interpolation of a multiplier by algorithm (P1*).

The same Taylor series-based estimations may be carried out for the L^2 error. Reporting only dominant terms in κ or h, we have

$$\|\lambda - \pi_h\lambda\|^2_{0,[a,a+h]} \leqslant |\lambda|^2_{1,\infty,\Gamma}\kappa^2\frac{h^3}{3} + |\lambda'\lambda''|_{0,\infty,\Gamma}h^4\frac{\kappa}{12} + |\lambda|^2_{2,\infty,\Gamma}\frac{h^5}{120} \tag{34}$$

Assuming the same probability of occurrence, the error estimates reads

$$\left\|\lambda - \pi_h\bar{\lambda}\right\|^2_{0,\Gamma} \leqslant |\lambda|^2_{1,\infty,\Gamma}\kappa^3\frac{h^2}{3} + |\lambda'\lambda''|_{0,\infty,\Gamma}h^3\frac{\kappa^2}{12} + |\lambda|^2_{2,\infty,\Gamma}h^4\frac{1}{120} \tag{35}$$

It can be inferred from estimate (35) that even if algorithm $P1^*$ is not fully *P1* strictly speaking, it decreases the size and occurrence of *P0* zones so drastically that the corresponding suboptimal error components—the first two terms in (35)–have a very low coefficient, and thus, the optimal component—the third term in (35)—becomes dominant unless extremely high refinement is considered. Therefore, an optimal rate of convergence of 2 for $\|\lambda - \pi_h\lambda\|_{0,\Gamma}$ is expected for usual refinements. On the contrary, the occurrence of large *P0* zones in the $P1^-$ algorithm suggests a predicted convergence rate of 1.

Finally, the choice of parameter κ in algorithm $P1^*$ has to be a compromise between the precision that implies a decrease in the coefficient of the suboptimal component in (35) and the necessity to keep the conditioning number reasonable for almost coincident nodes. The conditioning number for a linear triangular element intersected with ratio $\kappa \ll 1$ at both edges is around κ^{-2}, as shown in [39] or [40]. In our calculations, $\kappa = 1.10^{-3}$ was adopted.

4. DESCRIPTION OF A CURVED GEOMETRY

We now consider problems where the interface may have any shape. Hence, a strategy to describe the interface geometry has to be introduced and assessed. The approach of Legay and coworkers [6] with curved quadratic triangles as subcells was chosen here. In an earlier paper [30], the accuracy of this description was quantified and extensively discussed. In this section, we recall the procedure and some important results about its accuracy.

4.1. Geometry description and approximation

As is usual with X-FEM, the exact interface location is implicitly known through a so-called level set function ϕ

$$\Gamma = \{\boldsymbol{x}, \phi(\boldsymbol{x}) = 0\} \tag{36}$$

Under the assumption that Γ has geometric continuity G^2, this means that for any point $\boldsymbol{x}$ in a 2δ-fixed width strip S_δ along the interface, we may define a unique projection point $\bar{\boldsymbol{x}}$ onto the interface (see Figure 15) as

$$\bar{\boldsymbol{x}} := \boldsymbol{x} - \phi(\boldsymbol{x})\nabla\phi(\boldsymbol{x}) \tag{37}$$

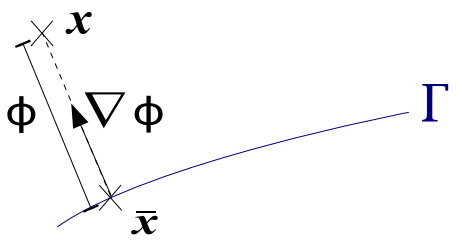

Figure 15. Properties of the level set function.

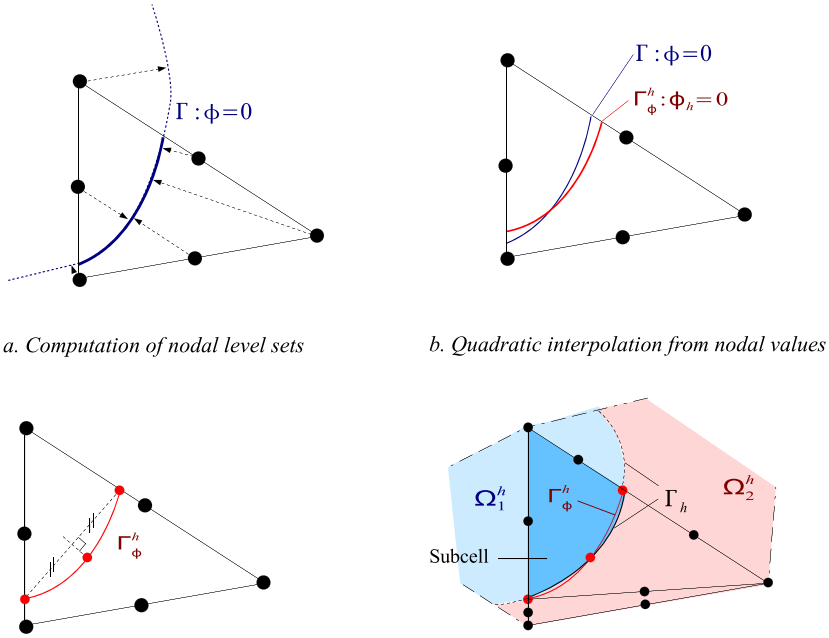

a. Computation of nodal level sets

b. Quadratic interpolation from nodal values

c. Determination of some points on the interpolated level-set isozero

d. Subdivision with corresponding quadratic triangles and approximated domains

Figure 16. Subdivision of cut elements in the case $g = 2$.

Appendix A of [30] may be consulted for a proof of this point and a definition of geometric continuity. Hence, ϕ is the signed distance to the interface and $\nabla\phi$, which verifies $|\nabla\phi| = 1$, and gives the normal direction to the interface at the projection point (see Figure 15).

We now aim at subdividing cut elements into quadrature subcells whose boundary would define an approximated interface location Γ_h. We consider the same family of triangulations, regarded as a finite element mesh of order $g \in \{1, 2\}$, which may be different from order p used for the field of unknowns.

Stage 1 of the geometry approximation.

In the first stage, the level set function itself is approximated by (see Figure 16b):

$$\phi_h(\boldsymbol{x}) = \sum_{j \in \mathcal{N}_h} N_j(\boldsymbol{x})\phi_j \tag{38}$$

where N_j is the shape function of order g associated with node j, and ϕ_j the values of the level set function at this node (see Figure 16a).

The need for a second stage.

Now, if $g = 1$, the zero isobar $\Gamma^h_\phi : \phi_h = 0$ is a broken line, so it may readily serve as boundary for linear conforming subcells. On the contrary, if $g = 2$, as in [6], iso-zero Γ^h_ϕ is constituted by conic sections element-wise. Now, subcells that would have such a curve as boundary are unusual. Hence, we would like to fit Γ^h_ϕ to the border of a quadratic subcell Γ_h, which is a parabola. This will be the purpose of our second stage.

Second stage of the geometry approximation.

In addition to both intersection points between Γ^h_ϕ and the edges of K, a middle point is determined using the perpendicular bisector to the segment between the previous points (see Figure 16c). Each cut element is then subdivided into quadratic triangular subcells (see Figure 16d), an edge of which interpolates the three points on the isozero curve. *This edge is finally the approximation* Γ_h *of the interface* (see Figure 16d).

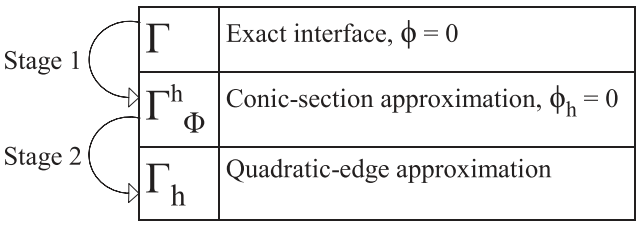

Figure 17. Approximation process of the geometry.

Figure 17 recaps the approximation process.

Hence, each subcell E is on a single side. We may then define approximated bodies Ω_i^h, as shown in Figure 16d.

4.2. Changes to the definition of the problem

Approximating domains change definition (19) of the Heaviside function to $H(\boldsymbol{x}) = \begin{cases} -1 \text{ if } \boldsymbol{x} \in \Omega_1^h \\ 1 \text{ if } \boldsymbol{x} \in \Omega_2^h \end{cases}$. Given expression (18) of the discrete space V_h, this implies that an interpolant $v_h \in V_h$ is discontinuous across Γ_h instead of Γ.

An immediate consequence is that the discrete solution u_h should not be compared with u as $\|u - u_h\|_{\Omega_1 \cup \Omega_2}$: this expression would not make sense. Indeed, as u_h is not continuous across Γ_h, it would be impossible to define ∇u_h there. Therefore, we should compare u_h with an extension $\bar{u}$ of u to be defined with a discontinuity across Γ_h instead of Γ, as $\|\bar{u} - u_h\|_{\Omega_1^h \cup \Omega_2^h}$.

To give full details about extension $\bar{u}$, let $\bar{\Omega}_i$ be a domain, which contains all discretizations Ω_i^h from a given mesh size and $\Omega_i : \forall h \leqslant h_0,\ \bar{\Omega}_i \subset \left(\Omega_i \cup \Omega_i^h\right)$. Let $u_i := u|_{\Omega_i}$ and assume $u_i \in H^{p+1}(\Omega_i)$. We may then extend u_i to $\bar{u}_i \in H^{p+1}\left(\bar{\Omega}_i\right)$ in a stable way (see Stein [41]). Extension $\bar{u} \in H^{p+1}\left(\Omega_h^1\right) \times H^{p+1}\left(\Omega_h^2\right)$ is then defined by combining the restrictions, as $\bar{u}|_{\Omega_h^i} := \bar{u}_i$.

Similarly, bulk bilinear forms a and a_h integrated on the *exact* or *approximated* domains are distinguished, as $a_h(v, w) := \sum_{i=1,2} \int_{\Omega_h^i} \left(\bar{\boldsymbol{A}}_i \cdot \nabla v\right) \cdot \nabla w dx$, $\bar{\boldsymbol{A}}$ being an extension to $\boldsymbol{A}$ abiding by the same paradigm as $\bar{u}$ instead of $a(u, v) := \sum_{i=1}^{2} \int_{\Omega_i} (\boldsymbol{A}_i \cdot \nabla u) \cdot \nabla v dx$ and so do linear forms l and l_h. Finally, bilinear forms to enforce the constraint should be distinguished between integrals over Γ or Γ_h as

$$\forall (u, \mu) \in V \times M, b(u, \mu) := \int_{\Gamma} \mu[u] d\Gamma \tag{39}$$

and

$$\forall (u_h, \mu_h) \in V_h \times M_h, b_h(u, \mu) := \int_{\Gamma_h} \mu_h[u_h] d\Gamma \tag{40}$$

This distinction is transmitted to the definition of the discrete multiplier space M_h, defined as the trace over Γ_h of functions in $\bar{M}_h$

$$M_h := \left\{\lambda_h|_{\Gamma h}, \lambda_h \in \bar{M}_h\right\} \tag{41}$$

4.3. About the accuracy of the geometrical representation

Let us now give some background evaluation from [30] about the accuracy of both approximation stages (see Table 17 and Figure 16). As for the first stage, it holds under regularity assumptions on Γ ([30], Lemma 4.1)

$$\forall j \in \{1..g+1\} \|\phi - \phi_h\|_{j,\infty,S_\delta} \leqslant C h^{g+1-j} \|\phi\|_{g+1,\infty,S_\delta} \tag{42}$$

About the second stage, writing an error to be assessed required a somewhat more elaborated methodology. We compared a polynomial mapping F_E that would map the reference triangle $\hat{K}$ onto the quadratic *triangular subcell* E (see Figure 18) to an analytical mapping $\tilde{F}_{\tilde{E}}$ that would map the reference triangle onto a subcell $\tilde{E}$ that would match Γ_ϕ^h perfectly (see Figure 18). Map $\tilde{F}_{\tilde{E}}$ is called *transfinite* and so is $\tilde{E}$, which are exclusively introduced for the sake of the demonstration. Under regularity assumptions about Γ, we proved that (see Appendix B of [30] for details)

$$\left\| \tilde{F}_{\tilde{E}} - F_E \right\|_{g+1,\infty,\hat{K}} \leqslant C\ (\hat{a}_M h)^{g+1} \tag{43}$$

where C includes quantities related to the regularity of Γ_ϕ^h.

4.4. Transfinite elements

Based on this construction, we may even build *transfinite elements*, which differ from transfinite subcells in the sense that $\hat{K}$ will this time be mapped onto a triangle $\tilde{K}$ « close to » K (see Figure 19) rather than onto $\tilde{E}$. Triangles $\tilde{K}$ should constitute a mesh where the interface is exactly resolved (see Figure 19). This turns out to be useful in the upcoming analysis, allowing the separation between interpolation and consistency errors.

So let K be a cut parent element. We are looking for a transfinite map $\tilde{F}_{\tilde{K}}$ that would map $\hat{K}$ onto a transfinite triangle $\tilde{K}$, in such a way that the affine pull back $\hat{\Gamma}$ of Γ_h be mapped onto Γ (see Figure 19). This condition is stated by the following theorem.

Theorem 4.1
For each non-slanted element $K \in \mathcal{E}_h$, a transfinite map $\tilde{F}_{\tilde{K}} : K \to \tilde{K}$ may be established, which observes the following properties:

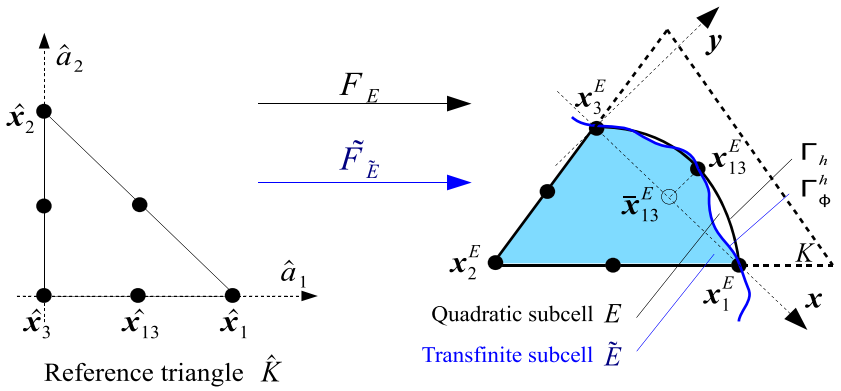

Figure 18. Classical and transfinite subcells, in the case where $g = 2$.

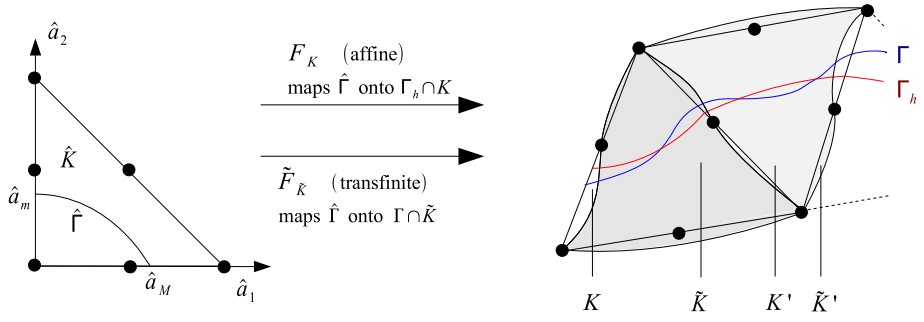

Figure 19. Transfinite elements and transfinite map.

(1) $\left(\tilde{K}\right)_{K\in\mathcal{T}_h}$ is an admissible mesh of Ω. In other terms, the intersection of two transfinite triangles $\tilde{K}\cap\tilde{K}'$ is either empty or equal to $\tilde{K}$ or reduces to an edge or a vertex (see Figure 19),
(2) $R_K := \tilde{F}_{\tilde{K}} - F_K$ verifies $\|R_K\|_{g+1,\infty,\hat{K}} \leqslant Ch^{g+1}$,
(3) $\tilde{F}_{\tilde{K}}^{-1}\left(\Gamma\cap\tilde{K}\right) = F_K^{-1}\left(\Gamma_h\cap K\right)$ (see Figure 19).

The proof of this theorem is rather technical and proposed in Appendix A.

4.5. Conforming discretization spaces over transfinite elements

For the sake of the error analysis, we will be led to define intermediate discretization spaces over transfinite elements. In this context, a discrete space of conforming fields is introduced as in [32]

$$\tilde{V}_h := \left\{v\in V, v|_{\tilde{K}\cap\Omega_i}\circ\tilde{F}_{\tilde{K}}\in P_p\left(\hat{K}\right)\right\} \tag{44}$$

Still following the guideline of [32], a map is then established between the elements of V_h and $\tilde{V}_h$ by letting $\mathcal{S}:\begin{cases}V_h\to\tilde{V}_h\\ v_h\to v_h\circ G_K\end{cases}$ and $\mathcal{C}=\mathcal{S}^{-1}:\begin{cases}\tilde{V}_h\to V_h\\ \tilde{v}_h\to\tilde{v}_h\circ G_K^{-1}\end{cases}$, where $G_K := F_K\circ\tilde{F}_{\tilde{K}}^{-1}$. In a similar way, the intermediate multiplier space is

$$\tilde{M}_h := \{J_t\mathcal{S}\mu_h,\ \mu_h\in M_h\} \tag{45}$$

where J_t is the dilatation induced by G_K in the tangential direction $\boldsymbol{t}$ to Γ

$$J_t := \left(\boldsymbol{t}^T\cdot DG_K^T\cdot DG_K\cdot\boldsymbol{t}\right)^{1/2} \tag{46}$$

It is then worth noticing that for $v_h\in V_h$ and $\mu_h\in M_h$,

$$\begin{aligned} b_h(v_h,\mu_h) &= \int_{\Gamma_h}[v_h]\mu_h ds \\ &= \int_{\Gamma}\left([v_h]\circ G_K\right)\left(\mu_h\circ G_K\right)J_t ds \\ &= b\left(\mathcal{S}[v_h], J_t\mathcal{S}\mu_h\right) \end{aligned} \tag{47}$$

Let us provide evaluations for the involved quantities. Because $\tilde{F}_{\tilde{K}} = F_K + R_K$, it follows that $G_K^{-1} = Id + R_K\circ F_K^{-1}$. It has been proven in Theorem 4.1 that $|R_K|_{0,\infty,\hat{K}}\leqslant Ch^{g+1}$, which implies $\left|G_K^{-1}-Id\right|_{0,\infty,K}\leqslant Ch^{g+1}$. In the same way, the Jacobian matrix of G_K^{-1} reads $DG_K^{-1} = I + \left[DR_K\circ F_K^{-1}\right]\cdot DF_K^{-1}$. Because $\left|DF_K^{-1}\right|_{0,\infty,K}\leqslant Ch^{-1}$, it satisfies $\left|DG_K^{-1}-I\right|_{0,\infty,K}\leqslant Ch^{g}$. As proven by Ciarlet (see [36], Theorem 4.3.3), when h is sufficiently small, the inverse G_K of G_K^{-1} satisfies

$$|G_K - Id|_{0,\infty,K}\leqslant Ch^{g+1} \tag{48}$$

$$|DG_K - I|_{0,\infty,K}\leqslant Ch^{g} \tag{49}$$

5. CONVERGENCE ANALYSIS WITH A WEAK DISCONTINUITY

Let us now analyze the convergence of the interface problem. To study the convergence with Lagrange multipliers, our key starting assumption is the stability of the discrete multiplier space. In X-FEM, this is classically translated by inf-sup condition (22) that becomes the following.

Assumption 5.1
The multiplier space abides by a discrete inf-sup condition, namely,

$$\exists c > 0,\ \forall \mu_h \in \tilde{M}_h,\ \sup_{v_h \in \tilde{V}_h} \frac{b(v_h, \mu_h)}{\|v_h\|_{1,\Omega_1 \cup \Omega_2}} \geqslant c h^{1/2} \|\mu_h\|_{0,\Gamma} \tag{50}$$

Let us point out that this condition is different from those usually admitted for mortar methods or standard FEM, where $h^{1/2}\|\mu_h\|_{0,\Gamma}$ is replaced with $\|\mu_h\|_{-1/2,\Gamma} \geqslant c h^{1/2}\|\mu_h\|_{0,\Gamma}$. So we have to figure out what to keep and what to rewrite from classical finite element proofs. In the end, the remarkable result is that it may indeed be proven that this inf-sup condition is sufficient to yield appropriate convergence, although it is a bit less stringent than those classically assumed.

5.1. Convergence analysis on transfinite elements

The first step of the convergence study consists in analyzing an « intermediate » interface problem relying on transfinite elements where the interface is, geometrically speaking, exactly resolved. This step is intended to produce interpolation-related errors while preventing any domain-related consistency error from appearing.

The intermediate discrete problem that we suggest to analyze reads: find $\left(\tilde{u}_h, \tilde{\lambda}_h\right) \in \tilde{V}_h \times \tilde{M}_h$ such as

$$\forall \tilde{v}_h \in \tilde{V}_h, a\left(\tilde{u}_h, \tilde{v}_h\right) + b\left(\tilde{v}_h, \tilde{\lambda}_h\right) = l\left(\tilde{v}_h\right) \tag{51}$$

$$\forall \tilde{\mu}_h \in \tilde{M}_h, b\left(\tilde{u}_h, \tilde{\mu}_h\right) = 0 \tag{52}$$

Because of a condition that $v|_{\Gamma_u^i} = 0$ in the definition of V, a verifies a coercivity assumption on V. Introducing the constrained space $V \supset \tilde{K}_h := \left\{\tilde{v}_h \in \tilde{V}_h, \forall \tilde{\mu}_h \in \tilde{M}_h, b\left(\tilde{v}_h, \tilde{\mu}_h\right) = 0\right\}$, the following error estimates hold for the intermediate discrete problem

Theorem 5.1
Extension to X-FEM of [32]*, Proposition 2.1.* Let u be the solution of the exact problem and λ be the corresponding normal flux, let $\tilde{u}_h$ be the solution of the intermediate discrete problem, then

$$\|u - \tilde{u}_h\|_{1,\Omega_1 \cup \Omega_2} \leqslant C \inf_{\tilde{v}_h \in \tilde{K}_h} \|u - \tilde{v}_h\|_{1,\Omega_1 \cup \Omega_2} + C \sup_{\tilde{w}_h \in \tilde{K}_h} \frac{b\left(\tilde{w}_h, \lambda\right)}{\|\tilde{w}_h\|_{1,\Omega_1 \cup \Omega_2}} \tag{53}$$

Moreover, if $\lambda \in L^2(\Gamma)$, then

$$\|u - \tilde{u}_h\|_{1,\Omega_1 \cup \Omega_2} \leqslant C \inf_{\tilde{v}_h \in \tilde{K}_h} \|u - \tilde{v}_h\|_{1,\Omega_1 \cup \Omega_2} + C h^{1/2} \inf_{\tilde{\mu}_h \in \tilde{M}_h} \|\lambda - \tilde{\mu}_h\|_{0,\Gamma} \tag{54}$$

Proof
The proof relies on the coercivity and continuity of a on V, on the expression of the intermediate and exact problem and on the definition of $\tilde{K}_h$. It is therefore strictly identical to proposition and Remark 2.6 in [42] for (53) from an original proof in [43]. The proof to obtain (54) from (53) comes from [32] and relies on the fact that $\forall \tilde{\omega}_h \in \tilde{V}_h, \|[\tilde{\omega}_h - \pi_h \tilde{\omega}_h]\|_{0,\Gamma} \leqslant C h^{1/2} \|\tilde{\omega}_h\|_{1,\Omega_1 \cup \Omega_2}$. Although this is a classical property of multiplier spaces with standard FEM, in our X-FEM case, it had to be explicitly proven in (31) by the dedicated Lemma 3.2. □

We now aim at estimating the first term of (54), making use of the nodal interpolation operators in the first stage (Lemma 5.1) and extending the results to the minimum over the restricted space in the second stage (Theorem 5.2) by taking advantage of the inf-sup condition. Let us introduce the following.

Definition 5.1
Let $u \in H^{p+1}(\Omega_1 \cup \Omega_2)$. We define a nodal interpolation operator by $\tilde{I}_p := \hat{I}_p \circ \tilde{F}_{\tilde{K}}^{-1}$ on $\tilde{K}$. We may then define an interpolation operator onto $\tilde{V}_h$ as in [24, 44] or [45] by $\tilde{\Pi}_h u|_{\Omega_i} = \tilde{I}_p \bar{u}_i$.

Lemma 5.1
Extension to X-FEM of [32]*, Lemma 2.3.* Let $u \in H^{p+1}(\Omega_1) \times H^{p+1}(\Omega_2)$, then $\left\|u - \tilde{\Pi}_h u\right\|_{1,\Omega_1\cup\Omega_2} \leqslant C h^p \|u\|_{p+1,\Omega_1\cup\Omega_2}$.

Proof
Extension to X-FEM of the proof in [32]. By letting $\hat{\bar{u}}_i := \bar{u}_i|_{\tilde{K}} \circ \tilde{F}_{\tilde{K}}$, we obtain

$$\left\|\hat{\bar{u}}_i - \hat{I}_p \hat{\bar{u}}_i\right\|_{1,\hat{K}} \leqslant C \left|\hat{\bar{u}}_i\right|_{p+1,\hat{K}} \leqslant C h^p \|\bar{u}_i\|_{p+1,K} \tag{55}$$

Transforming the left-hand side of (55) back to $\tilde{K}$ and using the concavity of the square root, we deduce $h^{-1}\left|\bar{u}_i - \tilde{I}_p \bar{u}_i\right|_{0,\tilde{K}} + \left|\bar{u}_i - \tilde{I}_p \bar{u}_i\right|_{1,\tilde{K}} \leqslant C h^p \|\bar{u}_i\|_{p+1,K}$, and the result follows by summation, definition of $\tilde{K}$ and stability of the extensions $\bar{u}_i$. □

In the upcoming developments, an estimate of the trace of this interpolation also comes out to be necessary. For this reason, we state the following lemma:

Lemma 5.2
The trace of the interpolation error abides by the following inequality. For $v \in V$,

$$\left\|\left[v - \tilde{\Pi}_h v\right]\right\|_{0,\Gamma} \leqslant C h^{p+1/2} \|v\|_{p+1,\Omega_1\cup\Omega_2} \tag{56}$$

Proof
With the notations of Figure 19 and denoting $\tilde{v}_h := \tilde{\Pi}_h v$ for the sake of convenience, we have $\|[v - \tilde{v}_h]\|_{0,\Gamma\cap\tilde{K}} = \left(\frac{\text{meas}(\Gamma\cap\tilde{K})}{\text{meas}(\hat{\Gamma})}\right)^{1/2} \left\|\left[\hat{v} - \hat{\tilde{v}}_h\right]\right\|_{0,\hat{\Gamma}}$ and $\frac{\text{meas}(\Gamma\cap\tilde{K})}{\text{meas}(\hat{\Gamma})} \leqslant C h$. Let us now consider the linear form $\Theta : \begin{cases} H^p\left(\hat{K}\right) \to \mathbb{R} \\ \hat{\varphi} \quad \to \int_{\hat{\Gamma}} \left(\left[\hat{v} - \hat{\tilde{v}}_h\right]\right)\left(\hat{\varphi} - \hat{I}_p\hat{\varphi}\right) ds \end{cases}$.

By virtue of the Schwarz inequality and the trace theorem, Θ is continuous, and the associated operator norm $\|\Theta\|^*$ satisfies $\|\Theta\|^* \leqslant C \left\|\left[\hat{v} - \hat{\tilde{v}}_h\right]\right\|_{0,\hat{\Gamma}}$. In this estimate, the constant in the trace theorem solely depends upon the Lipschitz constant of the domain formed by $\hat{\Gamma}$ and the boundaries of $\hat{K}$. Hence, because there is no slanted triangle, C is independent of K.

Let us now apply the Bramble–Hilbert lemma (see Section 3.1 of [36]), which is because that Θ is continuous and vanishes over $P_p\left(\hat{K}\right)$ and states that $|\Theta(\hat{\varphi})| \leqslant C \|\Theta\|^* |\hat{\varphi}|_{p+1,\hat{K}}$. Applying this result with the specific choice $\hat{\varphi} = \hat{\tilde{v}}_1 - \hat{\tilde{v}}_2$, whose trace on $\hat{\Gamma}$ verifies $\hat{\varphi}|_{\hat{\Gamma}} = [\hat{v}]$, and simplifying by $\left\|\left[\hat{v} - \hat{\tilde{v}}_h\right]\right\|_{0,\hat{\Gamma}}$, it comes $\left\|\left[\hat{v} - \hat{\tilde{v}}_h\right]\right\|_{0,\hat{\Gamma}} \leqslant C \left|\hat{\tilde{v}}_1 - \hat{\tilde{v}}_2\right|_{p+1,\hat{K}}$.

Pulling these quantities back onto the physical space, summing up the results and appealing to the stability properties of the extensions, it comes that $h^{-1/2}\|[v - \tilde{v}_h]\|_{0,\Gamma} \leqslant C h^p \|\bar{v}_1 - \bar{v}_2\|_{p+1,\Omega_1\cup\Omega_2}$. Applying this result to $p = 0$ gives $\|[v - \tilde{v}_h]\|_{0,\Gamma} \leqslant C h^{1/2} \|\bar{v}_1 - \bar{v}_2\|_{1,\Omega_1\cup\Omega_2}$. The stability of the extensions finally yields the result. □

The interpolation estimates may now be extended to the infimum over the constrained space.

Theorem 5.2
Extension to X-FEM of [32]*, Proposition 2.2.* The estimate for the lower bound over $\tilde{V}_h$ given in Lemma 5.2 also holds over the constrained space $\tilde{K}_h$, namely,

$$\inf_{v_h \in \tilde{K}_h} \|u - v_h\|_{1,\Omega_1 \cup \Omega_2} \leqslant C h^p \|u\|_{p+1,\Omega_1 \cup \Omega_2} \tag{57}$$

Proof
In this proof, we aim at correcting $\tilde{\Pi}_h u$ to cancel out its jump while keeping a similar estimate. We call $\tilde{z}$ the $L^2(\Gamma)$ projection of $\left[\tilde{\Pi}_h u\right]$ onto $\tilde{M}_h$, that is to say that the multiplier $\tilde{z} \in \tilde{M}_h$ such that $\forall \mu \in \tilde{M}_h$, $\int_\Gamma \left(\tilde{z} - \left[\tilde{\Pi}_h u\right]\right) \mu ds = 0$. Let then $w_h \in \tilde{V}_h$ be the displacement introduced in the proof of Theorem 1, which fulfills the inf-sup condition $\frac{b(w_h, \tilde{z})}{\|w_h\|_{1,\Omega_1 \cup \Omega_2}} \geqslant c h^{1/2} \|\tilde{z}\|_{0,\Gamma}$ and $\tilde{z} = [w_h]$. These properties and the definition of $\tilde{z}$ lead to

$$\|w_h\|_{1,\Omega_1 \cup \Omega_2} \leqslant C h^{-1/2} \frac{b\left(\tilde{\Pi}_h u, \tilde{z}\right)}{\|\tilde{z}\|_{0,\Gamma}} \tag{58}$$

The Schwarz inequality reads $b\left(\tilde{\Pi}_h u, \tilde{z}\right) \leqslant \left\|\left[\tilde{\Pi}_h u\right]\right\|_{0,\Gamma} \|\tilde{z}\|_{0,\Gamma}$, so that $\|w_h\|_{1,\Omega_1 \cup \Omega_2} \leqslant C h^{-1/2} \left\|\left[\tilde{\Pi}_h u\right]\right\|_{0,\Gamma}$. Because $[u] = 0$, we may write $\left[\tilde{\Pi}_h u\right] = \left[\tilde{\Pi}_h u - u\right]$. By virtue of Lemma 5.2, $\left\|\left[\tilde{\Pi}_h u - u\right]\right\|_{0,\Gamma} \leqslant C h^{p+1/2} \|u\|_{p+1,\Omega_1 \cup \Omega_2}$, which leads to $\|w_h\|_{1,\Omega_1 \cup \Omega_2} \leqslant C h^p \|u\|_{p+1,\Omega_1 \cup \Omega_2}$. Considering the particular choice $v_h = \tilde{\Pi}_h u - w_h \in \tilde{K}_h$ in the inferior bound, a triangle inequality yields $\inf_{v_h \in \tilde{K}_h} \|u - v_h\|_{1,\Omega_1 \cup \Omega_2} \leqslant \left\|u - \tilde{\Pi}_h u\right\|_{1,\Omega_1 \cup \Omega_2} + \|w_h\|_{1,\Omega_1 \cup \Omega_2}$. The conclusion then follows immediately by virtue of Lemma 5.1. □

As for the error on the Lagrange multiplier, the following error estimate holds.

Lemma 5.3
Provided $\lambda \in L^2(\Gamma)$, there exists C such that

$$\left\|\lambda - \tilde{\lambda}_h\right\|_{-1/2,\Gamma} \leqslant C \quad h^{1/2} \inf_{\mu_h \in \tilde{M}_h} \|\lambda - \mu_h\|_{0,\Gamma} + \|u - \tilde{u}_h\|_{1,\Omega_1 \cup \Omega_2} \Bigg) \tag{59}$$

Proof
Provided the inf-sup conditions (50) and (56), we apply Theorem 4.8 of [33] to prove (59). □

5.2. Convergence analysis on the actual elements

Carrying out the analysis on actual elements, the idea is to come down to the estimates of the previous conforming analysis to which only geometry-related *consistency* errors should be added.

By letting then $u'_h := \mathcal{S} u_h, \lambda'_h := J_t \mathcal{S} \lambda_h$ and $a'_h\left(\tilde{w}_h, \tilde{v}_h\right) := a_h\left(\mathcal{C}\tilde{w}_h, \mathcal{C}\tilde{v}_h\right)$, the discrete problem may be reformulated in

$$\forall \tilde{v} \in \tilde{V}_h,\ a'_h\left(u'_h, \tilde{v}\right) + b\left(\tilde{v}, J_t \lambda'_h\right) = l_h\left(\mathcal{C}\tilde{v}\right) \tag{60}$$

$$\forall \tilde{\mu} \in \tilde{M}_h,\ b\left(u'_h, J_t \tilde{\mu}\right) = 0 \tag{61}$$

We have the general estimate.

Lemma 5.4
Provided $\lambda \in L^2(\Gamma)$, the following estimates hold

$$\begin{aligned} \left\|u - u'_h\right\|_{1,\Omega_1 \cup \Omega_2} \leqslant C \inf_{v_h \in \tilde{K}_h} \|u - v_h\|_{1,\Omega_1 \cup \Omega_2} + \sup_{w_h \in \tilde{K}_h} \frac{a(v_h, w_h) - a'_h(v_h, w_h)}{\|w_h\|_{1,\Omega_1 \cup \Omega_2}} \Bigg) \\ + C \inf_{\mu_h \in \tilde{M}_h} h^{1/2} \|\lambda - \mu_h\|_{0,\Gamma} + \sup_{w_h \in \tilde{K}_h} \frac{l(w_h) - l_h(C w_h)}{\|w_h\|_{1,\Omega_1 \cup \Omega_2}} \end{aligned} \tag{62}$$

Proof
Very classical proof that consists in using the first Strang lemma together with Theorem 5.1. It is for instance identical to Proposition 2.16 of [42]. □

The first term in the right-hand side in (62) has already been assessed in Theorem 5.2 by (61). The third term is related to the interpolation error of the multiplier and will be estimated by Lemma 5.7. Regarding the second and fourth terms in (62), these consistency errors are estimated by the following.

Lemma 5.5
(From [32]*, Propositions 2.4 and 2.5)*. Let us recall that $g \in \{1, 2\}$ is the order of description of the interface, the second and fourth terms in (62) are, respectively, bounded by $O(h^g)$ and $O(h^{g+1})$.

Proof
The proof is a straightforward extension to the case $g = 2$ of [32]. It is not recalled for the sake of conciseness. □

The error in the Lagrange multiplier is now assessed for this discrete problem.

Lemma 5.6
Extension to X-FEM of [32]*, Proposition 2.4*. The error of the Lagrange multiplier is given by

$$\left\|\lambda - \lambda'_h\right\|_{0,\Gamma} \leqslant C$$
$$\left\{ \inf_{\mu_h \in \tilde{M}_h} \|\lambda - \mu_h\|_{0,\Gamma} + h^{-1/2} \left(\left\|u - u'_h\right\|_{1,\Omega_1\cup\Omega_2} + h^g \left(1 + \|u\|_{1,\Omega_1\cup\Omega_2}\right) + h^p \|u\|_{p+1,\Omega_1\cup\Omega_2} \right) \right\} \tag{63}$$

Proof
Once again, it is analogous to that in [32] except for subtleties due to using inf-sup condition (50) instead of a classical $H^{-1/2}(\Gamma)$ norm uniform inf-sup condition as in [32].

Step 1. With the inf-sup condition, it holds $\left\|\tilde{\lambda}_h - \lambda'_h\right\|_{0,\Gamma} \leqslant C h^{-1/2} \sup_{w_h \in \tilde{V}_h} \frac{b\left(w_h, \tilde{\lambda}_h - \lambda'_h\right)}{\|w_h\|_{1,\Omega_1\cup\Omega_2}}$, whose numerator is split into $b\left(w_h, \tilde{\lambda}_h - \lambda'_h\right) = b\left(w_h, \tilde{\lambda}_h - \lambda\right) + b\left(w_h, \lambda - \lambda'_h\right)$.

Step 2. Estimating $\sup_{w_h \in \tilde{V}_h} \frac{b\left(w_h, \tilde{\lambda}_h - \lambda\right)}{\|w_h\|_{1,\Omega_1\cup\Omega_2}}$.

We have $\sup_{w_h \in \tilde{V}_h} \frac{b\left(w_h, \tilde{\lambda}_h - \lambda\right)}{\|w_h\|_{1,\Omega_1\cup\Omega_2}} \leqslant \sup_{w \in V} \frac{b\left(w, \tilde{\lambda}_h - \lambda\right)}{\|w\|_{1,\Omega_1\cup\Omega_2}} = \left\|\tilde{\lambda}_h - \lambda\right\|_{-1/2,\Gamma}$. Lemma 5.3 then states that $\left\|\lambda - \tilde{\lambda}_h\right\|_{-1/2,\Gamma} \leqslant C \left(h^{1/2} \inf_{\tilde{\mu}_h \in \tilde{M}_h} \|\lambda - \tilde{\mu}_h\|_{0,\Gamma} + \|u - \tilde{u}_h\|_{1,\Omega_1\cup\Omega_2} \right)$. As for $\|u - \tilde{u}_h\|_{1,\Omega_1\cup\Omega_2}$, Theorem 5.1 gives $\|u - \tilde{u}_h\|_{1,\Omega_1\cup\Omega_2} \leqslant C \inf_{v_h \in \tilde{K}_h} \|u - v_h\|_{1,\Omega_1\cup\Omega_2} + C h^{1/2} \inf_{\mu_h \in \tilde{M}_h} \|\lambda - \mu_h\|_{0,\Gamma}$, the first term of which is finally estimated by Theorem 5.2, as $\inf_{v_h \in \tilde{K}_h} \|u - v_h\|_{1,\Omega_1\cup\Omega_2} \leqslant C h^p \|u\|_{p+1,\Omega_1\cup\Omega_2}$.

Step 3. Estimating $\sup_{w_h \in \tilde{V}_h} \frac{b(w_h, \lambda - \lambda'_h)}{\|w_h\|_{1,\Omega_1\cup\Omega_2}}$.

Subtracting the discrete problem (60) to the continuous one (13), one obtains $b\left(w_h, \lambda - \lambda'_h\right) = l(w_h) - l_h(\mathcal{C} w_h) + a'_h\left(u'_h, w_h\right) - a(u, w_h)$. We finally decompose $a'_h\left(u'_h, w_h\right) - a(u, w_h) = a\left(u'_h - u, w_h\right) + \left(a'_h - a\right)\left(u'_h w_h\right)$. Appealing to the continuity of a and the estimates of Lemma 5.5, it may be concluded that

$$\sup_{w_h \in \tilde{V}_h} \frac{b\left(w_h, \lambda - \lambda_h'\right)}{\|w_h\|_{1,\Omega_1 \cup \Omega_2}} \leqslant C h^g \left(1 + \left\|u_h'\right\|_{1,\Omega_1 \cup \Omega_2}\right) + C \left\|u - u_h'\right\|_{1,\Omega_1 \cup \Omega_2}$$

By writing $\left\|u_h'\right\|_{1,\Omega_1 \cup \Omega_2} \leqslant \|u\|_{1,\Omega_1 \cup \Omega_2} + \left\|u - u_h'\right\|_{1,\Omega_1 \cup \Omega_2}$ for h small enough, we have

$$\sup_{w_h \in \tilde{V}_h} \frac{b\left(w_h, \lambda - \lambda_h'\right)}{\|w_h\|_{1,\Omega_1 \cup \Omega_2}} \leqslant C h^g (1 + \|u\|_{1,\Omega_1 \cup \Omega_2}) + C \left\|u - u_h'\right\|_{1,\Omega_1 \cup \Omega_2}$$

Step 4. The expected result follows from combining the results of Steps 1–3 and remarking that $\left\|\tilde{\lambda}_h - \lambda_h'\right\|_{0,\Gamma} \geqslant \left\|\lambda - \lambda_h'\right\|_{0,\Gamma} - \left\|\tilde{\lambda}_h - \lambda\right\|_{0,\Gamma}$. □

We may then evaluate the following.

Lemma 5.7
Suppose $\lambda \in H^1(\Gamma)$, then the interpolation error over the Lagrange multiplier is

$$\inf_{\mu \in \tilde{M}_h} \|\lambda - \mu\|_{0,\Gamma} \leqslant \|\lambda - \pi_h \lambda\|_{0,\Gamma} + C h^g \|\lambda\|_{1,\Gamma} \tag{64}$$

The regularity of λ is related to that of u given that $\lambda := (\boldsymbol{A} \cdot \nabla u) \cdot \boldsymbol{n}$.

Proof
Because $\mathcal{S}(\pi_h \lambda) \in \tilde{M}_h$, $\inf_{\mu \in \tilde{M}_h} \|\lambda - \mu\|_{0,\Gamma} \leqslant \|\lambda - \mathcal{S}(\pi_h \lambda)\|_{0,\Gamma}$, which may be decomposed into

$$\|\lambda - \mathcal{S}(\pi_h \lambda)\|_{0,\Gamma} \leqslant \|\lambda - \pi_h \lambda\|_{0,\Gamma} + \|\pi_h \lambda - \mathcal{S}(\pi_h \lambda)\|_{0,\Gamma} + \|1 - J_t\|_{0,\infty,\Gamma} \|\pi_h \lambda\|_{0,\Gamma} \tag{65}$$

The second term may be split into $\|\pi_h \lambda - \mathcal{S}(\pi_h \lambda)\|_{0,\Gamma}^2 = \sum_{\tilde{K}} \|\pi_h \lambda - \mathcal{S}(\pi_h \lambda)\|_{0,\Gamma \cap \tilde{K}}^2$. We may then assert that $\|\pi_h \lambda - \mathcal{S}(\pi_h \lambda)\|_{0,\Gamma \cap \tilde{K}} \leqslant h \|\pi_h \lambda - \mathcal{S}(\pi_h \lambda)\|_{0,\infty,\Gamma \cap \tilde{K}}$ and make use of the Taylor inequality to evaluate $\|\pi_h \lambda - \mathcal{S}(\pi_h \lambda)\|_{0,\infty,\Gamma \cap \tilde{K}} \leqslant |\pi_h \lambda|_{1,\infty,\tilde{K}} \|G_K - Id\|_{0,\infty,\Gamma}$. The equivalence of all norms on the finite dimensional space of affine functions over the reference element yields $|\pi_h \lambda|_{1,\infty,\tilde{K}} \leqslant C h^{-1} |\pi_h \lambda|_{1,\tilde{K}}$. Combining those results yields

$$\|\pi_h \lambda - \mathcal{S}(\pi_h \lambda)\|_{0,\Gamma} \leqslant C |\pi_h \lambda|_{1,\mathcal{E}_h} \|G_K - Id\|_{0,\infty,\Gamma} \tag{66}$$

After Lemma 3.1, we have $|\pi_h \lambda|_{1,\mathcal{E}_h} \leqslant C h^{1/2} \|\lambda\|_{1,\Gamma}$. Because $\|G_K - Id\|_{0,\infty,K} \leqslant C h^{g+1}$, it holds

$$\|\pi_h \lambda - \mathcal{S}(\pi_h \lambda)\|_{0,\Gamma} \leqslant C h^{g+3/2} \|\lambda\|_{1,\Gamma} \tag{67}$$

Given the expression (47) that $J_t := \left(\boldsymbol{t}^T \cdot DG_K^T \cdot DG_K \cdot \boldsymbol{t}\right)^{1/2}$ and estimate (48) that $|DG_K - 1|_{0,\infty,K} \leqslant C h^g$ and the Taylor expansion of the square root, it follows immediately that

$$|J_t - 1|_{0,\infty,\hat{K}} \leqslant C h^g \tag{68}$$

Moreover, after Lemma 3.1 (L^2 stability), we have

$$\|\pi_h \lambda\|_{0,\Gamma} \leqslant C \|\lambda\|_{0,\Gamma} \tag{69}$$

Then, estimate (64) to be proven is deduced from (65) by replacing its second term with (67) and its third term with (68) and (69). □

We are now in position to conclude with the final usual estimates.

Theorem 5.3
Assume $u \in W^{1,\infty}(\Omega_1 \cup \Omega_2)$, the following a priori estimate holds for the displacement error

$$\begin{aligned}\|\bar{u} - u_h\|_{1,\Omega_1^h \cup \Omega_2^h} \leqslant C \Big\{ & h^p \|u\|_{p+1,\Omega_1 \cup \Omega_2} + h^{1/2} \|\lambda - \pi_h \lambda\|_{0,\Gamma} \\ & + h^g \left(1 + \|u\|_{1,\Omega_1 \cup \Omega_2}\right) + h^{g+1/2} \|\lambda\|_{1,\Gamma} \Big\}\end{aligned} \tag{70}$$

Proof Step 1. Given estimate (49) of $G_K - Id$, it holds

$$c \, \|\bar{u} - u_h\|_{1,\Omega_1^h \cup \Omega_2^h} \leqslant \left\|\mathcal{S}\bar{u} - u_h'\right\|_{1,\Omega_1 \cup \Omega_2} \leqslant C \, \|\bar{u} - u_h\|_{1,\Omega_1^h \cup \Omega_2^h} \tag{71}$$

This can be broken down into

$$\left\|\mathcal{S}\bar{u} - u_h'\right\|_{1,\Omega_1 \cup \Omega_2} \leqslant \|\mathcal{S}\bar{u} - u\|_{1,\Omega_1 \cup \Omega_2} + \left\|u - u_h'\right\|_{1,\Omega_1 \cup \Omega_2} \tag{72}$$

Step 2. The second term $\left\|u - u_h'\right\|_{1,\Omega_1 \cup \Omega_2}$ of (72) is assessed with Lemma 5.4 by estimation (62), whose first term $\inf_{v_h \in \tilde{K}_h} \|u - v_h\|_{1,\Omega_1 \cup \Omega_2}$ is bounded in Theorem 5.2 by $C h^p \|u\|_{p+1,\Omega_1 \cup \Omega_2}$, the second and fourth terms are evaluated by Lemma 5.5 as $\sup_{v \in \tilde{V}_h} \sup_{w \in \tilde{V}_h} \frac{a(v,w) - a_h'(v,w)}{\|w\|_{1,\Omega_1 \cup \Omega_2} \|v\|_{1,\Omega_1 \cup \Omega_2}} \leqslant C h^g$ and $\sup_{w_h \in \tilde{K}_h} \frac{l(w_h) - l_h(\mathcal{C} w_h)}{\|w_h\|_{1,\Omega_1 \cup \Omega_2}} \leqslant C h^{g+1}$ and the third term $h^{1/2} \inf_{\mu \in \tilde{M}_h} \|\lambda - \mu\|_{0,\Gamma}$ is bounded in Lemma 5.7 by $h^{1/2} \|\lambda - \pi_h \lambda\|_{0,\Gamma} + C h^{g+1/2} \|\lambda\|_{1,\Gamma}$.

Step 3. The first term of (72) is exclusively because of the approximation of the geometry. Let us call S_h the part of the domain which is in $\left(\Omega_1 / \Omega_1^h\right) \cup \left(\Omega_1^h \backslash \Omega_1\right)$: it is basically the domain enclosed by $\Gamma_h \cup \Gamma$ (see Figure 20). It holds $|\mathcal{S}\bar{u} - u|^2_{1,\Omega_1 \cup \Omega_2} = |\mathcal{S}\bar{u} - u|^2_{1,(\Omega_1 \cup \Omega_2) \backslash S_h} + |\mathcal{S}\bar{u} - u|^2_{1,S_h}$. Because $\bar{u} = u$ on $\Omega \backslash S_h$, we have $|\mathcal{S}\bar{u} - u|^2_{1,(\Omega_1 \cup \Omega_2) \backslash S_h} = \int_{(\Omega_1 \cup \Omega_2) \backslash S_h} \nabla\left(\mathcal{S}\bar{u} - u\right) \cdot \nabla\left(\mathcal{S}\bar{u} - \bar{u}\right) d\Omega$. Moreover, $|\mathcal{S}\bar{u} - u|^2_{1,S_h} = \int_{S_h} \nabla\left(\mathcal{S}\bar{u} - u\right) \cdot \nabla\left(\mathcal{S}\bar{u} - \bar{u}\right) d\Omega + \int_{S_h} \nabla\left(\mathcal{S}\bar{u} - u\right) \cdot \nabla\left(\bar{u} - u\right) d\Omega$. Let us sum up these results.

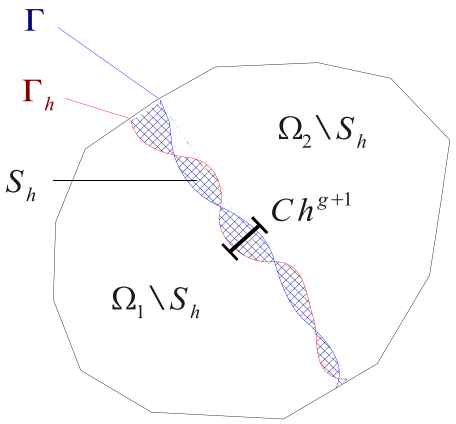

Figure 20. Exact and approximate domains.

$$|\mathcal{S}\bar{u}-u|^2_{1,\Omega_1\cup\Omega_2} \leqslant \int_{\Omega_1\cup\Omega_2} \nabla\left(\mathcal{S}\bar{u}-u\right)\cdot\nabla\left(\mathcal{S}\bar{u}-\bar{u}\right)d\Omega + \int_{S_h} \nabla\left(\mathcal{S}\bar{u}-u\right)\nabla\left(\bar{u}-u\right)d\Omega \tag{73}$$

The first term at the right-hand side of (73) may be bounded by $Ch^g\,|\mathcal{S}\bar{u}-u|_{1,\Omega_1\cup\Omega_2}$ with Schwarz inequality and the very same argument about $G_K - Id$ as in Step 1. As for the second term of (73), it may be bounded by $Ch^{g+1}\|u\|_{1,\infty,\Omega_1\cup\Omega_2}\,|\mathcal{S}\bar{u}-u|_{1,\Omega_1\cup\Omega_2}$ because the width of S_h is $O(h^{g+1})$ after Theorem 4.1 and $\text{meas}(S_h) \leqslant Ch^{g+1}\text{meas}(\Gamma)$ (Figure 20).

Then $|\mathcal{S}\bar{u}-u|_{1,\Omega_1\cup\Omega_2} \leqslant Ch^g(1+h\|u\|_{1,\infty,\Omega_1\cup\Omega_2})$ or for h sufficiently small, $|\mathcal{S}\bar{u}-u|_{1,\Omega_1\cup\Omega_2} \leqslant Ch^g$. Repeating the proof for the L^2 norm and scalar product brings $\|\mathcal{S}\bar{u}-u\|_{0,\Omega_1\cup\Omega_2} \leqslant Ch^g$, hence,

$$\|\mathcal{S}\bar{u}-u\|_{1,\Omega_1\cup\Omega_2} \leqslant Ch^g \tag{74}$$

□

Theorem 5.4
The following a priori estimates hold for the multiplier error.

$$\begin{aligned}\|\lambda-\lambda_h\|_{0,\Gamma} \leqslant C\Big\{&\|\lambda-\pi_h\lambda\|_{0,\Gamma} + h^g\|\lambda\|_{1,\Gamma}\\ &+h^{-1/2}\left(\|\bar{u}-u_h\|_{1,\Omega_1^h\cup\Omega_2^h} + h^g\left(1+\|u\|_{1,\Omega_1\cup\Omega_2}\right) + h^p\|u\|_{p+1,\Omega_1\cup\Omega_2}\right)\Big\}\end{aligned} \tag{75}$$

Proof
The estimate is split into $\left\|\lambda-\lambda'_h\right\|_{0,\Gamma}$ and $\left\|\lambda'_h-\lambda_h\right\|_{0,\Gamma}$. By virtue of Lemmas 5.6 and 5.7, the first is estimated by

$$\begin{aligned}\left\|\lambda-\lambda'_h\right\|_{0,\Gamma} \leqslant\ & C\|\lambda-\pi_h\lambda\|_{0,\Gamma}\\ &+h^{-1/2}\left\{\left\|u-u'_h\right\|_{1,\Omega_1\cup\Omega_2} + h^g(1+\|u\|_{1,\Omega_1\cup\Omega_2}) + h^g\|\lambda\|_{1,\Gamma} + h^p\|u\|_{p+1,\Omega_1\cup\Omega_2}\right\}\end{aligned}$$

We may then split $\left\|u-u'_h\right\|_{1,\Omega_1\cup\Omega_2} \leqslant \|u-\mathcal{S}\bar{u}\|_{1,\Omega_1\cup\Omega_2} + \left\|\mathcal{S}\bar{u}-u'_h\right\|_{1,\Omega_1\cup\Omega_2}$, for which $\left\|\mathcal{S}\bar{u}-u'_h\right\|_{1,\Omega_1\cup\Omega_2} \leqslant C\,\|\bar{u}-u_h\|_{1,\Omega_1^h\cup\Omega_2^h}$ (see (71)) and $\|\mathcal{S}\bar{u}-u\|_{1,\Omega_1\cup\Omega_2} \leqslant Ch^g$ after (74). As for $\left\|\lambda'_h-\lambda_h\right\|_{0,\Gamma}$, it holds $\left\|\lambda'_h-\lambda_h\right\|_{0,\Gamma} \leqslant Ch^{g+3/2}\|\lambda\|_{1,\Gamma}$ arguing as in Lemma 5.7, given that $\lambda'_h = J_t\mathcal{S}\lambda_h$. □

5.3. About the optimal convergence orders

Before we check those results against numerical experiments, let us mention some points which are likely to improve our theoretical prediction

- As pointed out by Melenk and Wohlmuth in [31], in the theoretical estimates for the dual variable, the displacement-related terms were found to be suboptimal when compared with experiments in numerous papers, down a factor $h^{1/2}$. The authors extensively discuss the issue in [31] and offer a proof that the missing factor may almost be theoretically recovered (in fact, a factor $h^{1/2}\log(h)$ may be recovered). This would allow to remove the highlighted factor $h^{-1/2}$ from (75).
- Second, when comparing our domain consistency error h^g from Lemma 5.5, obtained with transfinite elements, to the domain consistency error $h^{g+1/2}$ from [30], obtained with a direct analysis, we may be led to think that our estimates are suboptimal, down $h^{1/2}$. Such a suboptimality was actually observed on all our numerical experiments. This would allow to replace term $h^g\left(1+\|u\|_{1,\Omega_1\cup\Omega_2}\right)$ in (70) and (75) by $h^{g+1/2}\left(1+\|u\|_{1,\Omega_1\cup\Omega_2}\right)$.

To sum it up, taking into account the aforementioned facts leads us to the following expected convergence orders, denoting $\mathcal{O}(.)$ Landau's notation for an asymptotic bounding function

$$\|\bar{u} - u_h\|_{1,\Omega_1^h \cup \Omega_2^h} = \mathcal{O}\left(h^p + h^{g+\frac{1}{2}}\right) + \mathcal{O}\left(h^{\frac{1}{2}} \|\lambda - \pi_h \lambda\|_{0,\Gamma}\right) \tag{76}$$

$$\|\lambda - \lambda_h\|_{0,\Gamma} = \mathcal{O}\left(\|\lambda - \pi_h \lambda\|_{0,\Gamma}\right) + \mathcal{O}(h^g) + \mathcal{O}\left(\|\bar{u} - u_h\|_{1,\Omega_1^h \cup \Omega_2^h}\right) \tag{77}$$

In the upcoming numerical experiments, keeping the origin of these terms in mind is crucial. It is especially useful to know in what particular cases their related errors vanish, in which case the term disappears from the estimate

- Term $\mathcal{O}(h^p)$ disappears when the interpolation basis owns the exact displacement.
- Term $\mathcal{O}\left(\|\lambda - \pi_h \lambda\|_{0,\Gamma}\right)$ disappears in case $\lambda \in M_h$, which holds true if the exact pressure is spanned by the basis. It is the case for a constant pressure for instance.
- Term $\mathcal{O}(h^{g+1/2})$ originating from term $h^{g+1/2}\left(1 + \|u\|_{1,\Omega_1 \cup \Omega_2}\right)$ in (70) and term $\mathcal{O}(h^g)$ originating from terms $h^g\left(1 + \|u\|_{1,\Omega_1 \cup \Omega_2}\right)$ in (75) are called *bulk consistency error*. They vanish if the interface is exactly resolved.
- Terms $\mathcal{O}(h^{g+1/2})$ and $\mathcal{O}(h^g)$, respectively, originating from term $h^{g+1/2}\|\lambda\|_{1,\Gamma}$ in (70) and $h^g\|\lambda\|_{1,\Gamma}$ in (75) are called *surface consistency error*. They are induced by the presence of Lagrange multipliers and vanish if the interface is exactly resolved or if $\lambda \in \tilde{M}_h$.

Let us now recapitulate the expected displacement and multiplier convergence rates for some combinations (the mentioned « exact » means that we consider a particular case whose exact solution belongs to the interpolation space).

As for the multiplier, the expected convergence rates are summarized on Tables I-II.

Table I. Expected convergence orders for the displacement in the energy norm.

Displacement	Multiplier space	Subdivision (Geometry representation order g)	Multiplier interpolation related error: order of $(\pi_h\lambda - \lambda) + 0,5$	Displacement interpolation error rate p	Geometry-related consistency: order $g + 0,5$	Energy error rate
P1	P1$^-$	P1	1,5 (1 + 0,5)	1	1,5 (1 + 0,5)	1
P1	P1*	(any)	No convergence (inf-sup condition is violated)			
P2	P1*	P1	2,5 (2 + 0,5)	2	1,5 (1 + 0,5)	1, 5
P2	P1$^-$	P2	1,5 (1 + 0,5)	2	2,5 (2 + 0,5)	1, 5
P2	P1*	P2	2,5 (2 + 0,5)	2	2,5 (2 + 0,5)	2
P1-exact	P1$^-$	P1	1,5 (1 + 0,5)	—	1,5 (1 + 0,5)	1, 5
P2-exact	P1*	P2	2,5 (2 + 0,5)	—	2,5 (2 + 0,5)	2, 5
P2	P1$^-$- exact	P2	—	2	2,5 (2 + 0,5)	2
P1	P1$^-$- exact	P1	—	1	1,5 (1 + 0,5)	1

Table II. Expected convergence orders for the displacement in the energy norm.

Displacement	Multiplier space	Subdivision (Geometry representation order g)	Multiplier interpolation error rate	Displacement related error rate	Geometry-related consistency error rate	Multiplier L^2-error rate
P1	P1$^-$	P1	1	1	1	1
P1	P1*	(any)	No convergence (inf-sup condition is violated)			
P2	P1*	P1	2	1,5	1	1
P2	P1$^-$	P2	1	1,5	2	1
P2	P1*	P2	2	2	2	2
P1-exact	P1$^-$	P1	1	1,5	1	1
P2-exact	P1*	P2	2	2,5	2	2
P2	P1$^-$- exact	P2	—	2	2	2
P1	P1$^-$- exact	P1	—	1	1	1

6. NUMERICAL RESULTS

6.1. Cracked block under cubic pressure

In this test, a square elastic block of side 1 m is clamped on its lower boundary. Third-order polynomial boundary conditions are prescribed, namely, a displacement $\boldsymbol{u}_a$ on the upper boundary and surface loads $\boldsymbol{g}_l$ and $\boldsymbol{g}_r$ on the side boundaries (see Figure 21)

$$\boldsymbol{u}_a = \frac{-1}{E}\left\{p_3 x^3 + p_2 x^2 + p_0\right\}\boldsymbol{y} \tag{78}$$

$$\boldsymbol{g}_l = -p_2 y(y-1)\boldsymbol{x} + \left\{p_3 y^2\left(y - \frac{3}{2}\right) + 5\frac{p_3}{16}\right\}\boldsymbol{y} \tag{79}$$

$$\boldsymbol{g}_r = (3p_3 + p_2)y(y-1)\boldsymbol{x} + \left\{-3\frac{p_3}{4} - \frac{p_2}{2} - p_3 y^2\left(y - \frac{3}{2}\right) - 5\frac{p_3}{16}\right\}\boldsymbol{y} \tag{80}$$

where $p_3 = 3.10^4 Pa/m^3$; $p_2 = 3.10^4 Pa/m^2$; $p_0 = 1.10^4 Pa$. This block is cut through by a straight 20° leaning adherent interface (see Figure 21). The coefficients of elasticity are $E = 10^{10} Pa$ and $\nu = 0$, so as to obtain an analytical solution easily. It reads

$$\sigma_{xx} = 3p_3 xy(y-1) + p_2 y(y-1) \tag{81}$$

$$\sigma_{yy} = -p_3 x^3 - p_2 x^2 - p_0 + 3p_3\frac{x}{2}\left(y - \frac{1}{2}\right) + \frac{p_2}{2}\left(y - \frac{1}{2}\right) \tag{82}$$

$$\sigma_{xy} = -3p_3\frac{x^2}{4} - p_2\frac{x}{2} - p_3 y^3 + 3p_3\frac{y^2}{2} - 5\frac{p_3}{16} \tag{83}$$

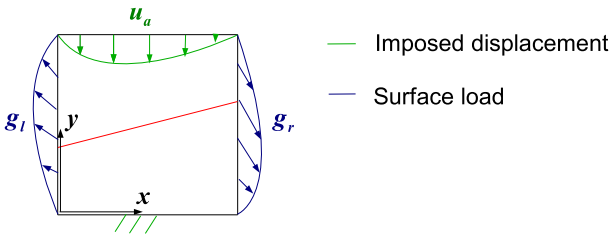

Figure 21. Block submitted to a cubic pressure.

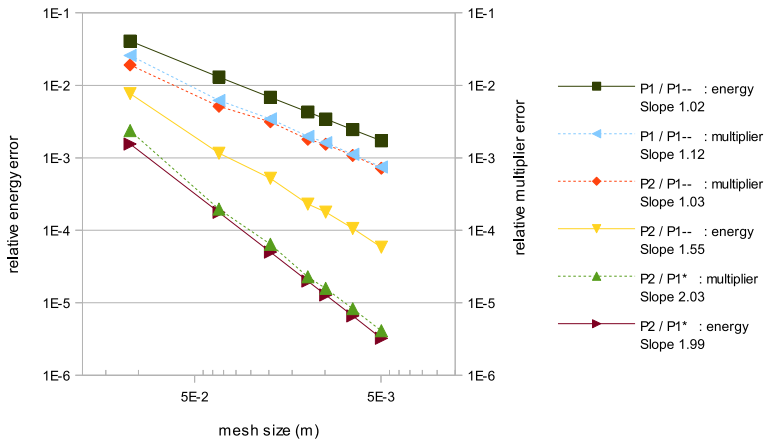

Figure 22. Convergence curves on energy and multipliers for the block under pressure.

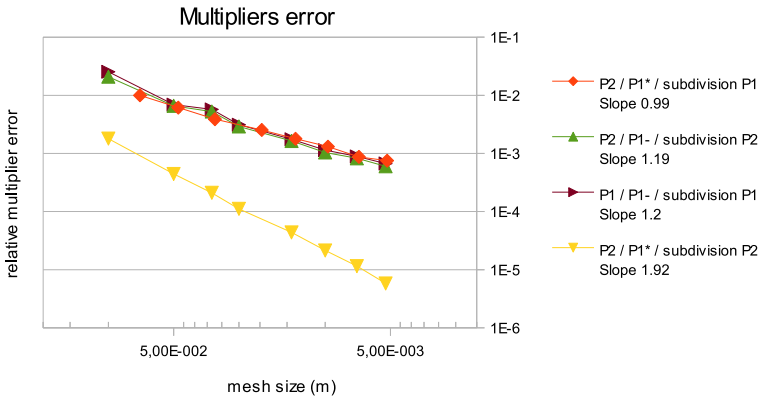

Figure 23. Circular inclusion under compressive loads.

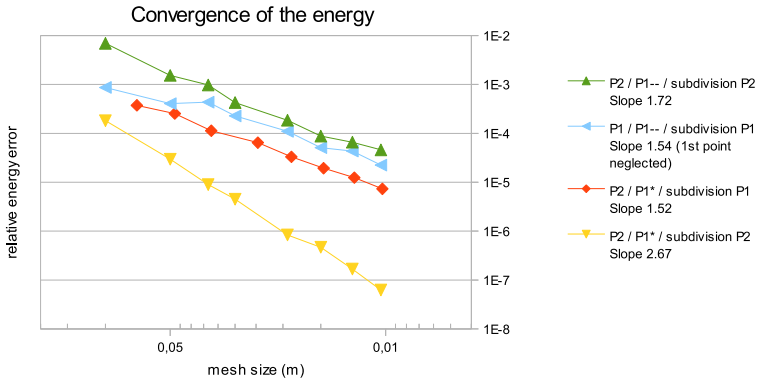

Figure 24. Circular inclusion under compressive loads: multiplier convergence.

Obviously, the interface is exactly resolved here, so the terms with g are removed from (76) and (77). The interpolation errors are the only remaining, so the test is well-suited to study the ability of the $P1^-$ and $P1^*$ algorithms to produce optimal orders of convergence. For linear interpolation of the displacement, and therefore $P1^-$ algorithm for the multipliers, well-known optimal orders around 1 are observed for the energy and multiplier errors. Using algorithm $P1^-$ together with a quadratic displacement yields suboptimal orders of convergence for the multipliers and the energy, close to 1 and 1.5, respectively, (see Figure 22), as predicted by the theory. Indeed, this suggests that the suboptimal term dominates in (35) due to large P0 zones in algorithm $P1^-$. Opting for algorithm $P1^*$ instead allows us to recover the optimal orders of accuracy 2 both in energy and multipliers, as illustrated by Figure 22.

6.2. Circular inclusion under compressive loads

We consider an elastic circular inclusion of radius 0,4 m embedded in a square block of side 1 m made of the same material. Coefficients of elasticity are $E = 100$ Pa and $\nu = 0$. A uniform pressure $p_1 = 2$ Pa is applied on the upper and lower boundaries, and a smaller pressure $p_2 = 1$ Pa is applied on the side boundaries (see Figure 23). Lateral motion is prevented on the middle nodes of those boundaries, so as to prevent rigid motion. Because the interface is adherent, the analytical solution is the one without inclusion $\boldsymbol{\sigma} = -p_1 \boldsymbol{y} \otimes \boldsymbol{y} - p_2 \boldsymbol{x} \otimes \boldsymbol{x}$. We point out that the exact displacement belongs to the interpolation basis in this test, so term p is removed from (76).

For $(P1/P1^-)$ interpolation, the convergence order is found out to be 1.2 for the multiplier and 1.54 for the energy when neglecting the coarser value (see Figures 24 and 25). The energy order of

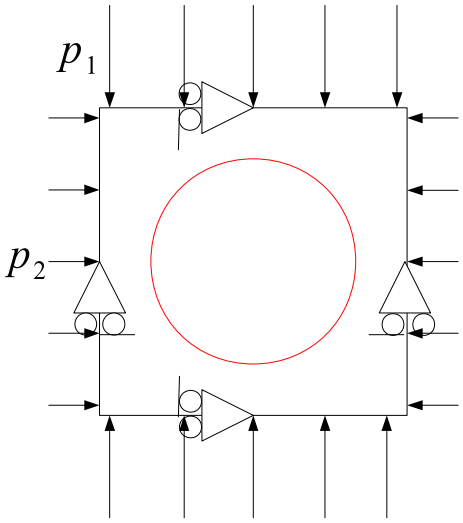

Figure 25. Circular inclusion under compressive loads: energy error.

convergence is close to the theoretical value 1.5 and above the theoretical value of 1. For the multiplier, possibly an effect of P1 zones in the $(P1)$ algorithm still tends to increase the observed order of convergence at low levels of refinement. More important, the results for $(P2/P1^*)$ interpolation with a linear description of the geometry confirm the predicted *surface consistency error*, with observed suboptimal slopes 0.99 and 1.52 for the multiplier and energy, respectively, close to the theoretical predictions 1 and 1.5 (see Figures 24 and 25).

A quadratic description of the geometry allows instead to recover the optimal orders of convergence. Once again, the observed values are in accordance with their theoretical counterparts 2 for the multiplier and 2.5 for the energy. Finally, the results for $(P2/P1)$ interpolation (with a quadratic description of the geometry) offer a new illustration of suboptimal rates with this set of discretizations, with an interpolation order of the multipliers at 1.19 slightly above 1, which triggers a roughly 0.5 higher order 1.72 for the energy, when 1.5 was expected.

6.3. Bimaterial ring

This numerical experiment aims at testing the ability of the Lagrange multipliers approach to deal with an actual interface problem. The reference model, which is available in [3] or [46], consists of an outer ring 1 that is made of material $E_1 = 10^9$ Pa and $\nu_1 = 0.3$ and geometrically delimited by radii $R_1 = 1$ m and $R_2 = 0,6$ m. It encloses an inner ring 2 of material properties $E_2 = 10^8$ Pa and $\nu_2 = 0.2$, which has an inner radius $R_3 = 0,2$ m (see Figure 26). The interface bonding the rings is adherent. A uniform external pressure $\sigma = 100$ Pa is applied on the outer boundary $r = R_1$, whereas the inner boundary $r = R_3$ is free.

An analytical solution in plane stress is available for this problem, for which the contact pressure on the interface $r = R_2$ is found to be

$$\lambda = \frac{2\sigma R_1^2}{R_1^2(1+\nu_1) + R_2^2(1-\nu_1) + \frac{E_1}{E_2}\frac{R_1^2-R_2^2}{R_2^2-R_3^2}\left(R_2^2(1-\nu_2) + R_3^2(1+\nu_2)\right)} \tag{84}$$

Introducing $A_1 = \frac{\lambda R_2^2 - \sigma R_1^2}{R_1^2-R_2^2}$, $B_1 = (\lambda-\sigma)\frac{R_1^2R_2^2}{R_1^2-R_2^2}$, $A_2 = -\lambda\frac{R_2^2}{R_2^2-R_3^2}$ and $B_2 = -\lambda\frac{R_2^2R_3^2}{R_2^2-R_3^2}$, the analytical displacement on ring i is

$$\boldsymbol{u} = u_i(r)\boldsymbol{e}_r = \frac{1}{E_i}\left\{(1-\nu_i)A_i r + (1+\nu_i)\frac{B_i}{r}\right\}\boldsymbol{e}_r \tag{85}$$

In the adaptation to X-FEM, a square with a side of 2 m is meshed. So as to account for external pressure, the analytical displacement is prescribed on the side of this mesh as a boundary condition.

The material interface and inner hole are represented by, respectively, adherent and free X-FEM interfaces (see Figure 26).

In this test, the exact pressure is constant along the interface. As a consequence, the interpolation error of the Lagrange multiplier may be removed from (76) and (77).

The results on multipliers and energy for the bimaterial test show optimal rates for P1 displacement and P1 subdivision, with convergence orders slightly above the theoretical value of 1, as well as for P2 displacement and P2 subdivision with experimental rates matching the theoretical value of 2 almost exactly (see Figure 27). This illustrates the ability of the method to optimally solve interface problems, including when higher-order interpolations are used.

The test was also run for a P2 displacement and P1 subdivision. The pressure converges at the suboptimal 0.98 rate, close to the prediction of 1 given by (77). However, the energy exhibits a superconvergent rate 1.88, where we would expect 1.5 (see Figure 27). As was done in [30], we highlight that the effect is partly because of symmetry compensations by randomly perturbing the geometry description within the $O(h^2)$ range predicted in Theorem 4.1. The expected rate 1.5 is then observed, illustrating the correctness of the prediction for the *bulk consistency error*.

6.4. A practical study of the problematic case of slanted triangles

We shall now discuss the case of *slanted* triangles, which were excluded from the demonstration of the inf-sup (Theorem 1) and examine whether it actually causes trouble or if it is only a technical issue of the demonstration. So we would like to see whether the constants of the convergence analysis—especially that of the inf-sup condition—are affected or not in the borderline case where ratio $\hat{a}_M/\hat{a}_m$ gets big, which indicates the presence of *slanted* triangles. We then consider the

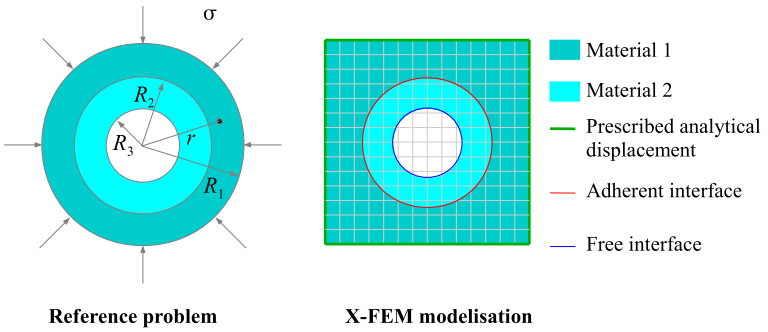

Figure 26. Bimaterial ring.

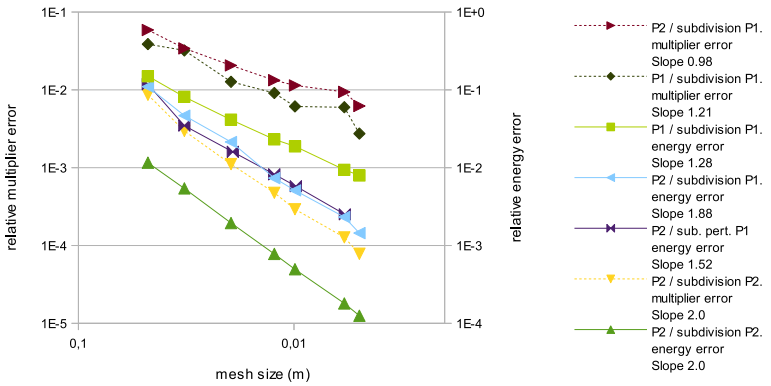

Figure 27. Convergence curves for a bimaterial ring.

cracked block test of Section 6.1 again and give it a small but nonzero leaning angle, so that slanted triangles will appear. The relative pressure error or local multiplier error is then plotted against ratio $\hat{a}_M/\hat{a}_m$ for the different triangles on Figure 28. No difference could be observed between slanted and other triangles, suggesting that the constants in the convergence analysis are not affected, and *the problem is more a shortcoming of the demonstration than a practical issue*.

7. CONCLUSION AND OUTLOOK

A Lagrange multiplier approach was adopted to deal with weak discontinuity problems. A new restriction algorithm $(P1^*)$ was proposed for the Lagrange multipliers in part 3, which is dedicated to a combined use with P2 displacements. A mathematical proof that it would then pass the inf-sup condition was presented. In part 4, an a priori error estimate was established for weak discontinuity problems for the H^1 norm of the displacement and L^2 norm of the Lagrange multiplier, as a function of the resolution of the interface and the interpolation error of the Lagrange and displacement spaces. It was checked against numerical experiments in part 5: when observed rates were above theoretical ones, this has been explained in light of what earlier literature says. We show, among other things, that the $(P1^*)$ algorithm and quadratic subdivision achieve quadratic convergence with a P2 displacement.

Considering extension at higher orders, estimates from Tables I–II suggest that a (Pk)-reduced multiplier space is natural for $(k+1)$-order X-FEM. For instance, a formulation $(P3-P2^*)$ would be worth studying, where $(P2^*)$ would be a space of piecewise quadratic multipliers on the major part of the interface Γ. However, finding a direct natural definition for $(P2^*)$ with Lagrange shape functions seems hard. A hierarchical basis should be used instead, in which shape functions with order $(p-1)$ or lower are conserved when defining the p-order finite element basis (see, e.g., [47]). In return, such hierarchical shape functions do not verify Kronecker's property of being 1 on one node and 0 on all others. As a result, instead of a nodal definition, a second-order hierarchical shape function is implemented with an associated DOF over an edge. As such, it may be viewed as an additional bubble function: middle nodes are still represented by gray circles in Figure 29 for the ease of representation, but this feature must be kept in mind.

Then, $(P2^*)$ is most naturally defined as an extension of $(P1^*)$: linear hierarchical DOF is related by applying $(P1^*)$, and additional equality relations are then prescribed between quadratic « bubble » functions (see Figure 29). A natural algorithm would consist in

(1) Assigning zero on the « bubble » DOF associated with the edges, which already support an equality relation in $(P1^*)$ or any non-intersected edge belonging to a triangle with a small intersection;
(2) Proceeding iteratively from there, triangle by triangle, by prescribing an equality relation between both edges not already having one.

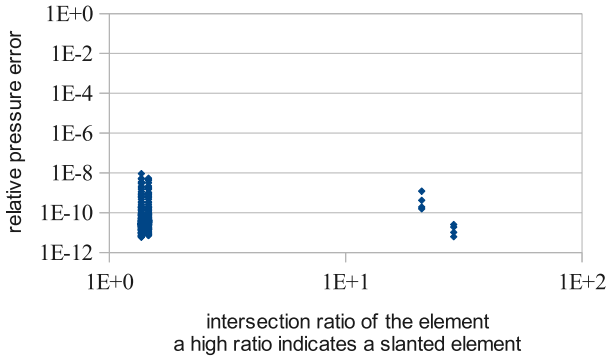

Figure 28. Cracked block: local pressure errors.

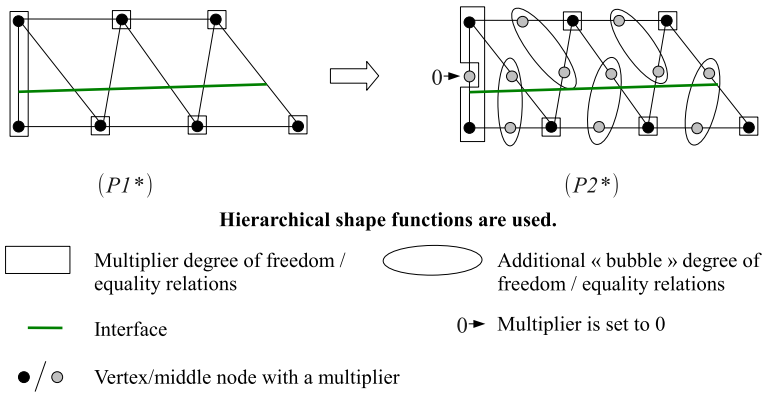

Figure 29. Constructing $(P2^*)$ from $(P1^*)$ with hierarchical shape functions: the case of an interface cutting the mesh far from vertices.

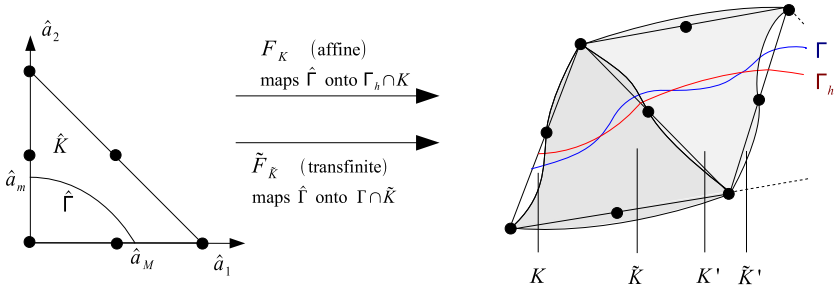

Figure A.1. Transfinite elements and transfinite map.

The case when the interface cuts the mesh far from vertices has been represented in Figure 29.

Given the variety of possible combinations for quadratic shape functions, proving non-redundancy appears more complicated than it was with $(P1^*)$: ensuring that nonzero combinations of bubble and linear functions never exhibit zero trace on the interface is not obvious.

To conclude, extending $(P1^*)$ to higher orders means handling additional « bubble » shape functions, which are either related to edges (second-order and above) or elements (third-order and above) instead of the nodal definition in $(P1^*)$. This change of properties explains why extending $(P1^*)$ to higher orders is not straightforward: new strategies have to be found to connect the associated DOFs.

APPENDIX A: PROOF OF THEOREM 4.1

The statement of the theorem is recalled hereafter

Theorem 7.1
For each non-slanted element $K \in \mathcal{E}_h$, a transfinite map $\tilde{F}_{\tilde{K}} : K \to \tilde{K}$ may be established, which observes the following properties:

(1) $\left(\tilde{K}\right)_{K \in \mathcal{T}_h}$ is an admissible mesh of Ω. In other terms, the intersection of two transfinite triangles $\tilde{K} \cap \tilde{K}'$ is either empty, or equal to $\tilde{K}$, or reduced to an edge or a vertex (see Figure A.1);
(2) $R_K := \tilde{F}_{\tilde{K}} - F_K$ verifies $\|R_K\|_{g+1,\infty,\hat{K}} \leqslant C h^{g+1}$;
(3) $\tilde{F}_{\tilde{K}}^{-1}\left(\Gamma \cap \tilde{K}\right) = F_K^{-1}\left(\Gamma_h \cap K\right)$ (see Figure A.1).

Proof
The process of geometry approximation involves two stages. It is extensively discussed in Section 4.1 and summarized in Figure 16. In one word, the first stage deduces a first approxima-

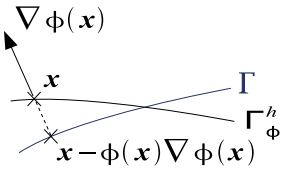

Figure A.2. Transfinite map: first step.

tion Γ_ϕ^h as the iso-zero of the discrete level set function. In the second stage, each cut element is subdivided into conforming quadratic subcells, an edge of which fits three points on Γ_ϕ^h. The set of all such edges constitutes Γ_h.

First stage of the construction.

A map $\tilde{F}_K^1$ is constructed in such a way that $G_K^1 := \tilde{F}_K^1 \circ F_K^{-1}$ maps Γ_ϕ^h onto Γ. An element $K \in \mathcal{E}_h$ is not invariant by G_K^1, but it is mapped onto a triangle with curved boundaries $\tilde{K}$ (see Figure A.1). Because Γ_ϕ^h has a poor regularity across the elements (as the case for Γ_h in Figure A.1), $\tilde{K}$ will be constructed such that $\Gamma_\phi^h \cap K$ be mapped onto $\Gamma \cap \tilde{K}$ so as to ensure sufficient regularity properties for G_K^1. Let $\boldsymbol{x} \in \Gamma_\phi^h$, then $\phi_h(\boldsymbol{x}) = 0$ (see Figure A.2). After (37), it holds $\boldsymbol{x} - \phi(\boldsymbol{x})\nabla\phi(\boldsymbol{x}) \in \Gamma$, so that $\boldsymbol{x} - (\phi(\boldsymbol{x}) - \phi_h(\boldsymbol{x}))\,\nabla\phi(\boldsymbol{x}) \in \Gamma$ (see Equation 37). Hence, $G_K^1 := (Id + [\phi_h - \phi]\nabla\phi)$ is adopted, so that $\tilde{F}_K^1$ is defined by means of

$$R_K^1 := \tilde{F}_K^1 - F_K := ([\phi_h - \phi]\nabla\phi) \circ F_K \tag{A.1}$$

The differentiation rule for composed functions is then used to differentiate (A.1). Provided that $|DF_K| \leqslant Ch$ and the higher-order derivatives of F_K are zero, assuming that ϕ and its derivatives are regular, and given that for $j \in \{0..g+1\}$, we have, according to (42), $\|\phi - \phi_h\|_{j,\infty,K} \leqslant Ch^{g+1-j}$; it becomes $\left\|R_K^1\right\|_{g+1,\infty,\hat{K}} \leqslant Ch^{g+1}$.

Second stage of the construction.

In this second stage, $\tilde{F}_K^2$ is created in such a way that $G_K^2 := \tilde{F}_K^2 \circ F_K^{-1}$ maps Γ_h onto Γ_ϕ^h, whereas the intersected edges of K remain invariant by this transformation (see Figure A.3).

The map for points located on the interface, when $g = 1$. In the case where $g = 1$, the pullback $\hat{\Gamma} := F_K^{-1}(\Gamma_h)$ is merely the segment $\hat{e}$ linking the pullbacks of the intersection points (see Figure A.3). To any point on $\hat{\Gamma}$, we may associate a coordinate $\hat{a} = \hat{a}_1/\hat{a}_M$ ranging from 0 to 1 along $\hat{e}$. For such points, $\tilde{F}_K^2$ is defined such that $R_{K,1}^2 := \tilde{F}_K^2 - F_K := R_E(\hat{a})\,\boldsymbol{y}$, where $R_E(\hat{a}) := \tilde{F}_{\tilde{E}}(\hat{a}, 0) - F_E(\hat{a}, 0)$ is the error between Γ_h and Γ_ϕ (Figure 18).

*The map for any point, when $g = 1$.*First, the map $R_{K,g=1}^2$ must be extended to the whole triangle in such a way that it will be zero on the pullbacks of the intersected edges. Hence, definition $\hat{a} = \hat{a}_1/\hat{a}_M$ may no longer be used, because it is not uniformly 1 along the edge $\{\hat{a}_2 = 0\}$. Instead, we set $\hat{a} := \frac{r\hat{a}_1}{\hat{a}_2 + r\hat{a}_1}$ with $r := \hat{a}_m/\hat{a}_M$. First, this reduces to $\hat{a}_1/\hat{a}_M$ on $\hat{e}$, because an equation of $\hat{e}$ is $\hat{e} : \hat{a}_2 + r\hat{a}_1 = \hat{a}_m$. Second, we do have $\hat{a} = 0$ along the edge $\{\hat{a}_1 = 0\}$ and $\hat{a} = 1$ along the edge $\{\hat{a}_2 = 0\}$ this time, implying that $R_E(\hat{a}) = 0$ along these edges. We then set $\tilde{F}_K^2$ such that

$$R_{K,1}^2 := \tilde{F}_K^2 - F_K := \left(\frac{\hat{a}_2 + r\hat{a}_1}{\hat{a}_m}\right)^{g+1} R_E(\hat{a})\,\boldsymbol{y} \tag{A.2}$$

In the previous expression, factor $\left(\frac{\hat{a}_2 + r\hat{a}_1}{\hat{a}_m}\right)^{g+1}$ is meant to recover the regularity properties demanded by *b)* as will be highlighted in the next step. This coefficient value is obviously 1 on $\hat{\Gamma}$.

The map for any point, when $g = 2$. A preliminary step has to be added, which maps $\hat{\Gamma}$ onto $\hat{e}$. Let us denote $\boldsymbol{y}$ and $\boldsymbol{Y}$, the second local axis of K and $\hat{K}$ and y_c and Y_c, the related coordinates at the summit of parabola Γ_h and $\hat{\Gamma}$ (see Figure A.3), we may define $\hat{F}(\hat{\boldsymbol{x}}) = \hat{\boldsymbol{x}} + 4\frac{\hat{a}_1\hat{a}_2}{\hat{a}_m\hat{a}_M} Y_c \boldsymbol{Y}$. It satisfies $\hat{F}(\hat{e}) = \hat{\Gamma}$ and we shall construct $R_{K,2}^2 = R_{K,1}^2 \circ \hat{F}^{-1}$, where the expression for $R_{K,1}^2$ is given by (A.2). We may evaluate y_c by applying (43) with $g = 1$ as $y_c = O\left(\hat{a}_M^2 h^2\right)$, so its pull back satisfies $Y_c = O\left(\hat{a}_M^2 h\right)$, and we can deduce that $\left|\hat{F} - Id\right|_{0,\infty,\hat{K}} \leqslant \frac{C}{rh} \leqslant Ch$ because

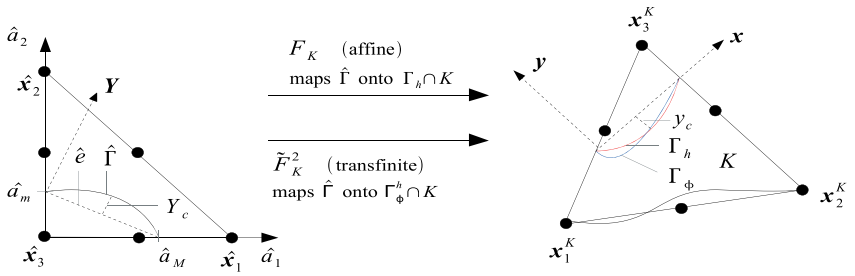

Figure A.3. Transfinite map: second step.

there are no slanted elements. Hence, when h is sufficiently small, $\hat{F}$ is invertible and the successive derivatives of $\hat{F}^{-1}$ are bounded, as shown by Ciarlet (see [36], Theorem 4.3.3). We may therefore denote $R_K^2 = R_{K,1}^2$ from here onward and study this map without loss of generality.

Proof that R_K^2 and its derivatives satisfy c). Equation (43) states that $\|R_E\|_{g+1,\infty,\hat{K}} \leqslant Ch^{g+1}\hat{a}_M^{g+1}$. Replacing $\hat{a}_m = r\hat{a}_M$ and because r is bounded away from 0 for *non-slanted* triangles, we have $\left(\frac{\hat{a}_2+r\hat{a}_1}{\hat{a}_m}\right)^{g+1} \leqslant \frac{C}{\hat{a}_M^{g+1}}$. The two previous results lead to $\left\|R_K^2\right\|_{0,\infty,\hat{K}} \leqslant Ch^{g+1}$. We aim at proving the same properties for the derivatives. Denoting D the derivation operator with respect to $\hat{\boldsymbol{x}}$ $(\hat{a}_1, \hat{a}_2)$ and considering $j \in \{1..g+1\}$, derivative $D^j R_K^2$ involved in (A.2) sums $\frac{d^l R_E}{d\hat{a}^l} \frac{1}{\hat{a}_m^{g+1}} D^{j-l}\left([\hat{a}_2 + r\hat{a}_1]^{g+1}\right) \otimes D^l\hat{a}$, where $l \in \{0..j\}$. The involved terms are estimated by $\|R_E\|_{g+1,\infty,\hat{K}} \leqslant Ch^{g+1}\hat{a}_M^{g+1}$, $\left|D^{j-l}\left([\hat{a}_2 + r\hat{a}_1]^{g+1}\right)\right| \leqslant |\hat{a}_2 + r\hat{a}_1|^{g+1-j+l}$ and the differentiation $\left|D^l\hat{a}\right| \leqslant \frac{r(l!)}{(\hat{a}_2+r\hat{a}_1)^l}$ of the definition of $\hat{\lambda}$. Hence, $\left|D^j R_K^2\right| \leqslant Ch^{g+1}\frac{1}{r^g}$, so if the element is not *slanted*, $\left\|R_K^2\right\|_{g+1,\infty,\hat{K}} \leqslant Ch^{g+1}$ is obtained.

Pulling together the results.

We shall now draw the conclusions of the theorem. Let us remind that we are looking for $\tilde{F}_{\tilde{K}}$ such that property *c)* $\tilde{F}_{\tilde{K}}^{-1}\left(\Gamma \cap \tilde{K}\right) = F_K^{-1}\left(\Gamma_h \cap K\right)$ be fulfilled. Applying $\tilde{F}_{\tilde{K}}$ to both sides, this amounts to seeking $G_K^{-1} := \tilde{F}_{\tilde{K}} \circ F_K^{-1}$ such that $\Gamma \cap \tilde{K} = G_K^{-1}\left(\Gamma_h \cap K\right)$. Because G_K^2 maps $\Gamma_h \cap K$ onto $\Gamma_\phi \cap K$ and G_K^1 maps $\Gamma_\phi \cap K$ onto $\Gamma \cap \tilde{K}$, we set

$$G_K^{-1} = G_K^1 \circ G_K^2 = \tilde{F}_K^1 \circ F_K^{-1} \circ \tilde{F}_K^2 \circ F_K^{-1} \tag{A.3}$$

Hence, the expression of $\tilde{F}_{\tilde{K}}$

$$\tilde{F}_{\tilde{K}} = \tilde{F}_K^1 \circ F_K^{-1} \circ \tilde{F}_K^2 \tag{A.4}$$

So property *c)* of the theorem holds by construction. Besides, let $(K', K) \in (\mathcal{E}_h)^2$ and $\boldsymbol{x} \in K \cap K'$, then $G_K^2(\boldsymbol{x}) = \boldsymbol{x}$. Moreover, $G_K^1(\boldsymbol{x})$ is composed of continuous functions depending upon the location of $\boldsymbol{x}$, but not upon K, so that the mapping is continuous across the elements boundaries: $G_K^1(\boldsymbol{x}) = G_{K'}^1(\boldsymbol{x})$. Hence, $G_K^{-1}(\boldsymbol{x}) = G_{K'}^{-1}(\boldsymbol{x})$. *Reductio ad absurdum*, this proves property *a)*: should there be any overlap or gap between neighboring transfinite triangles $\tilde{K}$ and $\tilde{K}'$, there would be a point $\boldsymbol{x} \in K \cap K'$ whose image by G_K^{-1} would be strictly inside or outside of $\tilde{K}'$, that is to say such that $G_K^{-1}(\boldsymbol{x}) \neq G_{K'}^{-1}(\boldsymbol{x})$, which is impossible.

Let us prove *b)*. The residual is $R_K = \left(F_K + R_K^1\right) \circ F_K^{-1} \circ \left(F_K + R_K^2\right) - F_K$, which can finally be reduced to

$$R_K = R_K^1 + R_K^1 \circ F_K^{-1} \circ R_K^2 + R_K^2 \tag{A.5}$$

Then the differentiation of (A.5) yields $\|R_K\|_{g+1,\infty,\hat{K}} \leqslant Ch^{g+1}$ according to the results of Steps 1 and 2 and the estimation $\left|DF_K^{-1}\right| \leqslant Ch^{-1}$. □

REFERENCES

1. Moës N, Dolbow J, Belytschko T. A finite element method for crack growth without remeshing. *International Journal for Numerical Methods in Enginnering* 1999; **46**:135–150.
2. Melenk JM, Babuˇska I. The partition of unity finite element method: basic theory and applications. *Computer Methods in Applied Mechanics and Engineering* 1996; **39**:289–314.
3. Sukumar N, Chopp DL, Moës N, Belytschko T. Modeling holes and inclusions by level-sets in the extended finite element method. *Computer Methods in Applied Mechanics and Engineering* 2001; **190**:6183–6200.
4. Moës N, Cloirec M, Cartraud P, Remacle JF. A computational approach to handle complex microstructure geometries. *Computer Methods in Applied Mechanics and Engineering* 2003; **192**:3163–3177.
5. Fries TP. A corrected XFEM approximation without problems in blending elements. *International Journal for Numerical Methods in Engineering* 2005; **64**:503–532.
6. Legay A, Wang H, Belytschko T. Strong and weak arbitrary discontinuities in spectral finite elements. *International Journal for Numerical Methods in Engineering* 2005; **64**:991–1008.
7. Chessa J, Wang H, Belytschko T. On the construction of blending elements for local partition of unity enriched finite elements. *International Journal for Numerical Methods in Engineering* 2003; **57**:1015–1038.
8. Gracie R, Wang H, Belytschko T. Blending in the extended finite element method by discontinuous galerkin and assumed strain methods. *International Journal for Numerical Methods in Engineering* 2008; **74**:1645–1669.
9. Cheng KW, Fries TP. Higher-order XFEM for curved strong and weak discontinuities. *International Journal for Numerical Methods in Engineering* 2010; **82**:564–590.
10. Zilian A, Legay A. The enriched space-time finite element method (est) for simultanous solution of fluid structure interaction. *International Journal for Numerical Methods in Engineering* 2008; **75**:305–334.
11. Diez P, Cottereau R, Zlotnik S. A stable XFEM formulation for multi-phase problems enforcing the accuracy of the fluxes through Lagrange multipliers. *International Journal for Numerical Methods in Engineering* 2013; **96**: 303–322.
12. Ji H, Dolbow J. On strategies for enforcing interfacial constraints and evaluating jump conditions with the extended finite element method. *International Journal for Numerical Methods in Engineering* 2004; **61**:2508–2535.
13. Mourad H, Dolbow J, Harari I. A bubble-stabilized finite element method for dirichlet constraints on embedded interfaces. *International Journal for Numerical Methods in Engineering* 2007; **69**:772–793.
14. Dolbow J, Franca L. Residual-free bubbles for embedded Dirichlet problems. *Computer Methods in Applied Mechanics and Engineering* 2008; **197**:3751–3759.
15. Sanders J, Dolbow J, Laursen T. On methods for stabilizing constraints over enriched interfaces in elasticity. *International Journal for Numerical Methods in Engineering* 2009; **78**:1009–1036.
16. Moës N, Béchet E, Tourbier M. Imposing Dirichlet boundary conditions in the extended finite element methods. *International Journal for Numerical Methods in Engineering* 2006; **67**:1641–1669.
17. Géniaut S, Massin P, Moës N. A stable 3D contact formulation for cracks using X-FEM. *Revue Européenne de Mécanique Numérique* 2007; **16**:259–276.
18. Béchet E, Moës N, Wohlmuth B. A stable Lagrange multiplier space for stiff interface conditions within the extended finite element method. *International Journal for Numerical Methods in Engineering* 2009; **78**:931–954.
19. Nitsche J. Ueber ein variationsprinzip zur loesung an Dirichlet-problemen bei verwendung von teilraeumen, die keinen randbedingungen entworfen sind. *Abhandlungen Aus Dem Mathematischen Seminar Der Universitat Hamburg* 1971; **36**:9–15.
20. Hansbo A, Hansbo P. An unfitted finite element method, based on nitscheś method for elliptic interface problems. *Computer Methods in Applied Mechanics and Engineering* 2002; **191**:5537–5552.
21. Hautefeuille M, Annavarapu C, Dolbow J. Robust imposition of dirichlet boundary conditions on embedded surfaces. *International Journal for Numerical Methods in Engineering* 2012; **90**:40–64.
22. Annaravapu C, Hautefeuille M, Dolbow J. A robust Nitscheś formulation for interface problems. *Computer Methods in Applied Mechanics and Engineering* 2012; **225**:44–54.
23. Haslinger J, Renard Y. A new fictious domain approach inspired by the extended finite element method. *SIAM Journal on Numerical Analysis* 2009; **47**:1474–1499.
24. Amdouni S, Hild P, Lleras V, Moakher M, Renard Y. A stabilized Lagrange multiplier method for the enriched finite-element approximation of contact problems of cracked elastic bodies. *Mathematical Modelling and Numerical Analysis* 2012; **49**:813–839.
25. Barbosa H, Hughes T. Finite element method with Lagrange multipliers on the boundary: circumventing the Babuska-Brezzi condition. *Computer Methods in Applied Mechanics and Engineering* 1991; **85**:109–128.
26. Stenberg R. On some techniques for approximating boundary conditions in the finite element method. *Journal of Computational and Applied Mathematics* 1995; **63**:139–148.
27. Pierrès E, Baietto M, Gravouil A. A two-scale extended finite element method for modelling 3D crack growth with interfacial contact. *Computer Methods in Applied Mechanics and Engineering* 2010; **199**:1165–1177.
28. Legrain G, Chevaugeon N, Dréau K. Higher-order X-FEM and levelsets for complex microstructures: uncoupling geometry and approximation. *Computer Methods in Applied Mechanics and Engineering* 2012; **241**:172–189.
29. Dréau K, Chevaugeon N, Moës N. Studied X-FEM enrichment to handle material interfaces with higher order finite element. *Computer Methods in Applied Mechanics and Engineering* 2010; **199**:1922–1936.
30. Ferté G, Massin P, Moës N. Convergence analysis of linear or quadratic X-FEM for curved free boundaries. *Computer Methods in Applied Mechanics and Engineering* 2014; **278**:794–827.

31. Melenk J, Wohlmuth B. Quasi-optimal approximation of surface based lagrange multipliers in finite element methods, Institute for Analysis and Scientific Computing, Vienna University of Technology: Vienna, 2011.
32. Flemisch B, Melenk J, Wohlmuth B. Mortar methods with curved interfaces. *Applied Numerical Mathematics* 2005; **54**:339–361.
33. Kikuchi N, Oden J. *Contact Problems in Elasticity. A Study of Variational Inequalities and Finite Element Methods*, Vol. 8. SIAM: Philadelphia, 1988.
34. Solberg J, Papadopoulos P. An analysis of dual formulations for the finite solution of two-body contact problems. *Computer Methods in Applied Mechanics and Engineering* 2005; **194**:2734–2780.
35. Clément P. Approximation by finite element functions using local regularization. *Revue Française Dáutomatique, Informatique, Recherche Opérationnelle* 1975; **9**:77–84.
36. Ciarlet P. *The Finite Element Method for Elliptic Problems*. North Holland: Amsterdam, 1979.
37. Attouch H, Buttazzo G, Michaille G. *Variational Analysis in Sobolev and BV Spaces: Application to PDE's and Optimization*. SIAM Series on Optimization: Philadelphia, 2006.
38. Chen Z, Nochetto R. Residual type a posteriori error estimates for elliptic obstacle problems. *Numerische Mathematik* 2000; **84**:527–548.
39. Siavelis M, Guiton M, Massin P. Large sliding contact along branched discontinuities in the X-FEM. *Computational Mechanics* 2013; **52**:201–219.
40. Géniaut S. Approche X-FEM pour la fissuration sous contact des structures industrielles. *Ph.D. Thesis*, Ecole Centrale de Nantes, Nantes, 2006.
41. Stein E. *Singular Integrals and Differenciability Properties of Functions*. Princeton University Press: Princeton, 1970.
42. Brezzi F, Fortin M. *Mixed and Hybrid Finite Elements Methods*, Springer Series in Computational Mathematics, vol. 15. Springer-Verlag: Berlin, 1991.
43. Babuska I. The finite element method with Lagrange multipliers. *Numerische Mathematik* 1973; **20**:179–192.
44. Nicaise S, Renard Y, Chahine E. Optimal convergence analysis for the extended finite element method. *International Journal for Numerical Methods in Engineering* 2010; **84**:1115–1138.
45. Chahine E, Laborde P, Renard Y. Crack tip enrichment in the XFEM method using a cut-off function. *International Journal for Numerical Methods in Engineering* 2008; **75**:629–646.
46. Li J, Melenk JM, Wohlmuth B. Optimal a priori estimates for higher order finite elements for elliptic interface problems. *Applied Numerical Mathematics* 2010; **60**:19–37.
47. Zienkiewicz O, Gago JDS, Kelly D. The hierarchical concept in finite element analysis. *Computers and Structures* 1983; **16**:53–65.